

UNCLASSIFIED

AD 4 2 3 0 9 5

DEFENSE DOCUMENTATION CENTER

FOR

SCIENTIFIC AND TECHNICAL INFORMATION

CAMERON STATION, ALEXANDRIA, VIRGINIA



UNCLASSIFIED

NOTICE: When government or other drawings, specifications or other data are used for any purpose other than in connection with a definitely related government procurement operation, the U. S. Government thereby incurs no responsibility, nor any obligation whatsoever; and the fact that the Government may have formulated, furnished, or in any way supplied the said drawings, specifications, or other data is not to be regarded by implication or otherwise as in any manner licensing the holder or any other person or corporation, or conveying any rights or permission to manufacture, use or sell any patented invention that may in any way be related thereto.

**PRESSURE FLUCTUATIONS RESULTING
FROM AN ALTERNATING FLOW SEPARATION
AND ATTACHMENT AT TRANSONIC SPEEDS**

By

H. L. Chevalier and J. E. Robertson
Propulsion Wind Tunnel Facility
ARO, Inc.

TECHNICAL DOCUMENTARY REPORT NO. AEDC-TDR-63-204

November 1963

AFSC Program Element 62405334/8953, Task 895307

(Prepared under Contract No. AF 40(600)-1000 by ARO, Inc.,
contract operator of AEDC, Arnold Air Force Station, Tenn.)

ARNOLD ENGINEERING DEVELOPMENT CENTER

AIR FORCE SYSTEMS COMMAND

UNITED STATES AIR FORCE

ORIGINAL AND TWO COPIES OF THIS REPORT
ARE TO BE DEPOSITED IN THE AEDC LIBRARY
AND THE AEDC INFORMATION CENTER
FOR THE AIR FORCE RESEARCH AND DEVELOPMENT
DIVISION, RANDOLPH AFB, TEXAS

NOTICES

Qualified requesters may obtain copies of this report from DDC, Cameron Station, Alexandria, Va. Orders will be expedited if placed through the librarian or other staff member designated to request and receive documents from DDC.

When Government drawings, specifications or other data are used for any purpose other than in connection with a definitely related Government procurement operation, the United States Government thereby incurs no responsibility nor any obligation whatsoever; and the fact that the Government may have formulated, furnished, or in any way supplied the said drawings, specifications, or other data, is not to be regarded by implication or otherwise as in any manner licensing the holder or any other person or corporation, or conveying any rights or permission to manufacture, use, or sell any patented invention that may in any way be related thereto.

ALL DDG
WHITE
SUGGESTIONS

PRESSURE FLUCTUATIONS RESULTING
FROM AN ALTERNATING FLOW SEPARATION
AND ATTACHMENT AT TRANSONIC SPEEDS

By

H. L. Chevalier and J. E. Robertson

Propulsion Wind Tunnel Facility

ARO, Inc.

a subsidiary of Sverdrup and Parcel, Inc.

November 1963

ARO Project No. PA2208

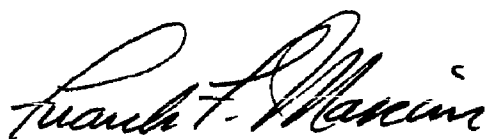
ABSTRACT

Investigations of unsteady pressures on cone-cylinder bodies at transonic Mach numbers were conducted in the Propulsion Wind Tunnel Facility (PWT). Static and unsteady pressure measurements were obtained for cone-cylinder bodies with cone half angles of 15, 20, 25, and 30 deg to determine characteristics of the various unsteady flow phenomena.

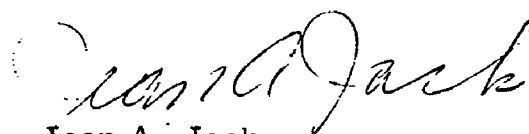
This report presents a detailed analysis of the alternating separation and attachment flow phenomenon that occurs at the shoulder of the cone-cylinder. Results of this analysis indicate that from the static pressure distributions, one may determine the regions of the model to be subjected to unsteady loads, the free-stream Mach number at which this will occur, and the peak-to-peak and root mean square amplitude of these loads. The magnitude of the pressure fluctuations ranges from 0 to 43 percent of the free-stream dynamic pressure, depending on cone angle, angle of attack, and position on the model surface, which correlates with predicted magnitudes from static pressure measurements.

PUBLICATION REVIEW

This report has been reviewed and publication is approved.



Frank F. Marvin
Lt Col, USAF
AF Representative, PWT
DCS/Test



Jean A. Jack
Colonel, USAF
DCS/Test

CONTENTS

	<u>Page</u>
ABSTRACT.	iii
NOMENCLATURE.	vii
1.0 INTRODUCTION	1
2.0 APPARATUS	
2.1 Test Facility.	1
2.2 Test Article	2
2.3 Instrumentation.	2
3.0 PROCEDURE	
3.1 Test Conditions.	3
3.2 Data Reduction	3
3.3 Precision of Measurements	4
4.0 RESULTS	4
4.1 Correlation of Static with Unsteady Pressures . .	6
4.2 Power Spectrum and Frequency Characteristics .	8
4.3 Comments on Alternating Flow Separation and Attachment.	9
4.4 Scale Effects.	10
4.5 Discussion.	10
5.0 CONCLUSIONS	11
REFERENCES	11

ILLUSTRATIONS

Figure

1.	Test Section of the 1-Foot Transonic Model Tunnel . .	13
2.	Details of the Cone-Cylinder Model	
a.	Model Dimensions	14
b.	Photograph of Model Components	15
3.	Model Installation.	16
4.	Details of the Pressure Transducer Mountings	
a.	Transducer Installations	17
b.	Reference Pressure System.	17
5.	Dynamic Response of the Model Transducer System Relative to a Flush-Mounted Transducer . . .	18
6.	Instrumentation for Data Recording	19

<u>Figure</u>		<u>Page</u>
7.	Variation of Reynolds Number with Mach Number. . .	20
8.	Variation of Dynamic Pressure with Mach Number . .	21
9.	Typical Time Sequence Photographs of the Alternating Separation and Attachment Flow Conditions at $M_\infty = 0.87$, 20-deg Cone Angle, Taken at 400 frames/sec.	23
10.	Variation of Pressure Coefficient with Mach Number for Various Angles of Attack, $x/D = 0.05$	
	a. $\theta_N = 15$ deg	25
	b. $\theta_N = 20$ deg	26
	c. $\theta_N = 25$ deg	27
	d. $\theta_N = 30$ deg	28
11.	Comparison of Pressure Distributions at Mach Numbers above and below the Mach Number Range of the Alternating Flow	
	a. $\theta_N = 15$ deg	29
	b. $\theta_N = 20$ deg	30
	c. $\theta_N = 25$ deg	31
	d. $\theta_N = 30$ deg	32
12.	Comparison of Static Peak-to-Peak Pressure Coefficients with Unsteady Peak-to-Peak Pres- sure Coefficients	
	a. $\theta_N = 15$ deg	33
	b. $\theta_N = 20$ deg	34
	c. $\theta_N = 25$ deg	35
	d. $\theta_N = 30$ deg	36
13.	Power Spectral Densities and Oscillograph Records of the Pressure Fluctuations at $x/D = 0.10$	
	a. $\theta_N = 20$ deg, $\alpha = 0$, $M_\infty = 0.87$	37
	b. $\theta_N = 25$ deg, $\alpha = -2$ deg, $M_\infty = 0.88$	38
	c. $\theta_N = 25$ deg, $\alpha = -4$ deg, $M_\infty = 0.87$	39
	d. $\theta_N = 30$ deg, $\alpha = -1$ deg, $M_\infty = 0.93$	40
	e. $\theta_N = 30$ deg, $\alpha = -2$ deg, $M_\infty = 0.91$	41

NOMENCLATURE

a	Amplitude of pressure fluctuation about the mean, psf
C_p	Pressure coefficient, $(p - p_\infty)/q_\infty$
ΔC_p	Change in pressure coefficient, $(C_{p1} - C_{p2})$
D	Maximum diameter of the model, ft
$F(\omega)$	Power spectral density, $\text{psf}^2/(\text{rad/sec})$
f	Frequency, cps
M_∞	Free-stream Mach number
p	Local static pressure, psf
Δp_f	Peak-to-peak pressure variation obtained from a flush-mounted transducer, psf
Δp_m	Peak-to-peak pressure variation obtained in calibration of the model transducer system, psf
p_t	Tunnel total pressure, psf
p_∞	Free-stream static pressure, psf
q_∞	Free-stream dynamic pressure, $\frac{\gamma}{2} p_\infty M_\infty^2$, psf
Re	Reynolds number, $\frac{V_\infty D}{\nu_\infty}$
t	Time, sec
V_∞	Free-stream velocity, ft/sec
x	Axial distance along model measured from cone-cylinder junction, ft
α	Angle of attack, deg
γ	Ratio of specific heats
θ_N	Nose cone half angle, deg
μ	The number of sign changes of $(p - p_{\text{ref}})$ per sec (see Section 4.2)
ν_∞	Kinematic viscosity of the free stream, ft^2/sec
ω	Circular frequency, $2 \pi f$, rad/sec

SUBSCRIPTS

1	Separated flow
2	Attached flow
∞	Free-stream conditions
ref	Mean static pressure used as a reference

1.0 INTRODUCTION

The use of cone-cylinders and cone-cylinder-flare combinations as boost and re-entry vehicles has created many problems of unsteady load conditions at transonic speeds. To provide some insight into these problems, a research investigation is being conducted at the Propulsion Wind Tunnel Facility (PWT), Arnold Engineering Development Center (AEDC), Air Force Systems Command (AFSC).

In the first phase of this investigation the nature of the background noise associated with the test facility, the Transonic Model Tunnel (TMT), was determined (Ref. 1). Concurrent tests were conducted on a 0.017-scale model of the Titan B Mark IV re-entry body (Ref. 2). The Titan test results indicated that four basic unsteady mechanisms may occur on a missile at transonic speeds. To determine the relationship of these mechanisms to model geometry, a systematic study was conducted in TMT to obtain both static and unsteady pressure measurements on cone-cylinder models with cone half angles of 10, 15, 20, 25, and 30 deg. The static pressure results are presented in Ref. 3.

This report presents a discussion of the general types of pressure fluctuations that were observed and gives a detailed description of the alternating flow separation and attachment phenomenon.

2.0 APPARATUS

2.1 TEST FACILITY

The Transonic Model Tunnel is a continuous-flow, open-circuit wind tunnel capable of operating at Mach numbers from 0.5 to 1.5. Mach numbers below 1.2 are obtained by the use of plenum suction in conjunction with a sonic nozzle contour. Mach numbers of 1.2 or greater are generated by a flexible plate nozzle, with plenum suction being used to stabilize flow in the test section. The test section, which is 12 by 12 in. in cross section and 37.5 in. in length, consists of four parallel perforated walls. Solid glass windows 11.75 in. long by 9.25 in. high were installed in the sidewalls so that schlieren pictures could be taken. These windows were present throughout the test. A more extensive description of the test facility is given in Ref. 4. Location of the model relative to the sting support system and details of the perforated walls used for the test are shown in Fig. 1.

Manuscript received August 1963.

2.2 TEST ARTICLE

Basic dimensions of the model and photographs of the various model components are shown in Figs. 2a and b, respectively. Axial distributions of the unsteady pressures were obtained using two pressure transducers by adding shims between the nose cone and the cylindrical portion of the model. Care was taken to obtain a flush fitting between the cone, shim, and cylinder to prevent discontinuities in the model surface. Figure 3 shows the model installed in the Transonic Model Tunnel.

2.3 INSTRUMENTATION

Two pressure transducers with a pressure range of ± 7.5 psid and a natural frequency of 7000 cps were housed inside the model. Flush-mounted transducers would have resulted in a discontinuity on the model surface; therefore each transducer was housed in a cavity. Installation of the transducers in the space available necessitated facing the transducers in opposite directions as shown in Fig. 4. The cavity for transducer 1 was connected to an orifice on the top surface of the model with approximately 0.75 in. of tubing, and the cavity for transducer 2 was connected to an orifice on the bottom surface of the model with approximately 1.75 in. of tubing. Each transducer was referenced to its dynamic cavity such that the reference pressure was the mean local pressure at the point where the unsteady pressure measurement was being made. Approximately 50 ft of tubing were used in the reference system for each transducer to ensure a steady reference pressure. Other details of the transducer installations are shown in Fig. 4.

The frequency response characteristics of the transducers, as installed, were determined as follows. A piston calibrator system was used to generate an approximate sinusoidal wave form at frequencies from 1 to 30 cps. Details of the calibrator are presented in Ref. 5. A flush-mounted transducer was used as a reference to determine pressures generated by the piston calibrator. The peak-to-peak pressure variation measured by the flush-mounted transducer was constant at 2.29 psi for frequencies from 1 to 30 cps. The model transducer system (Fig. 4) was connected to the calibrator and the outputs recorded over the same frequency range. The amplitude response of the model system relative to the flush-mounted transducer, $\frac{\Delta p_m}{\Delta p_f}$, is presented in Fig. 5. Below 10 cps, the amplitude response of the two transducers was approximately the same, whereas above 10 cps, the amplitude response of transducer 1 was greater than that of transducer 2. This difference apparently was caused by the different length tubes used to connect the transducers to the orifices. For

the alternating separation and attachment phenomenon described in this report, the frequency range of greatest interest is from 1 to 10 cps. In this range, the model system had a relative response greater than 85 percent for both transducer installations.

During the test, outputs from the transducers were recorded on magnetic tape and on an oscillograph. They were also monitored with a true root mean square (rms) voltmeter and an oscilloscope. Figure 6 shows the data recording and monitoring instrumentation. A schlieren system was used to obtain still and motion pictures of the flow about the model. The motion pictures were taken at 400 frames per second.

3.0 PROCEDURE

3.1 TEST CONDITIONS

Unsteady pressure data were obtained from the windward and leeward sides of the model at Mach numbers from 0.5 to 1.10 over a model angle-of-attack range of 0 to +6 deg. Unsteady pressure data obtained from the windward side of the model are presented as negative angle-of-attack data, and those obtained from the leeward side of the model are presented as positive angle-of-attack data. The Reynolds number and dynamic pressure ranges of the test are presented in Figs. 7 and 8, respectively. Static pressures were recorded from the reference lead of the transducers. These data are not presented; however, they were compared with the static data taken from Ref. 3 to ensure that correlation of static and dynamic data were made for the same local flow condition. All static pressure data presented herein were obtained from the test results discussed in Ref. 3.

3.2 DATA REDUCTION

Oscillograph records were obtained for each test condition. From these records the change in pressure coefficient, ΔC_p , for each unsteady flow condition was obtained. The oscillograph records were also analyzed for comparison with experimental power spectrums as explained in Section 4.2. The power spectral densities were obtained with a wave analyzer from selected data recorded on magnetic tape.

3.3 PRECISION OF MEASUREMENTS

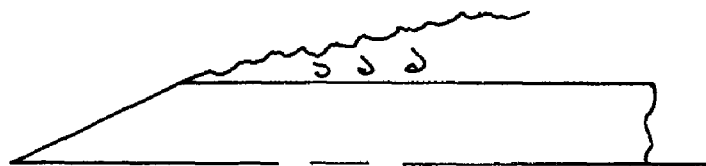
The uncertainty in Mach number determined by a statistical method based on a 95-percent confidence level and normal error distribution is ± 0.003 . The Mach number precision is based on the uncertainties involved in computing an average Mach number in the test section. Maximum variations from the average Mach number in the region of the model ranged from ± 0.004 at subsonic Mach numbers to ± 0.008 at $M_\infty = 1.15$. An estimate of the uncertainty in the free-stream dynamic pressure, q_∞ , is ± 6.0 psf. The flow angularity in the pitch plane of the test section for the Mach number range of the test is estimated to be 0.5 deg upflow. Data presented herein are not corrected for this flow angularity.

The uncertainty in the peak-to-peak pressure variations results from the dynamic response of the transducer system (see Section 2.3) and the inaccuracy of measuring the outputs from oscillograph records. This uncertainty is estimated to be up to 15 percent of the change in pressure for positive angle-of-attack data and up to 35 percent of the change in pressure for negative angle-of-attack data.

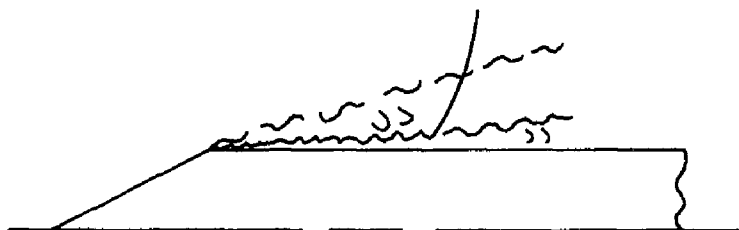
Uncertainties in the power spectral densities result from statistical errors in analyzing a finite data sample length and dynamic response errors of the transducer system. The sample length used was approximately one minute, and the scanning filter band width was 1.25 cps. For these conditions, one has a 95-percent confidence level that the power spectral densities have a value between 0.80 and 1.30 of the true mean. The uncertainty in the change in pressure resulting from the dynamic response of the transducer system ranges up to 15 percent of the true change in pressure for frequencies below 10 cps and up to 35 percent of the true change in pressure for frequencies above 10 cps. Thus the total uncertainty in the power spectral densities calculated according to the "law of the propagation of errors" ranges up to 35 percent for frequencies below 10 cps and up to 45 percent for frequencies above 10 cps.

4.0 RESULTS

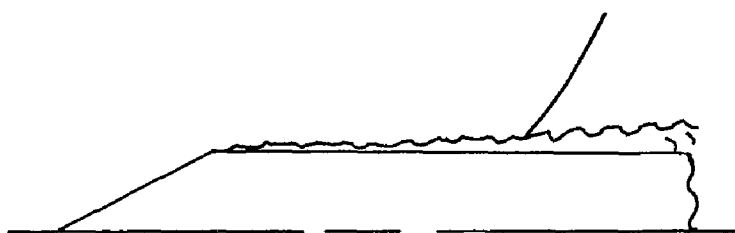
The results of this phase of the investigation showed four basic types of flow conditions that produce pressure fluctuations on cone-cylinder bodies at free-stream Mach numbers below 1.0. These were also noted in Ref. 2. Schematics of these flow conditions are shown on the following page.



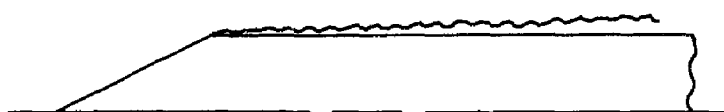
a. Separated Flow



b. Alternating Flow Separation and Attachment



c. Shock Wave Oscillation



d. Attached Flow

Although all four of these systems can produce pressure fluctuations on a body surface simultaneously, the flow fields shown in the schematics represent various ranges of free-stream Mach number. For low subsonic Mach numbers the flow is separated aft of the shoulder (A). As the Mach number is increased, the flow becomes attached at the shoulder and a shock wave appears on the cylinder (C). As the Mach number approaches 1.0, the shock wave moves downstream (D). The alternating flow condition (B) occurs in an intermediate Mach number range between A and C. The Mach number range associated with each flow condition depends on cone angle, angle of attack, and model scale.

The alternating flow condition is the most severe of the four basic types of unsteady flow conditions. The peak-to-peak pressures are large and cover a large area of the model surface. Only this flow condition will be discussed in this report. Time sequence schlieren photographs of this mechanism are shown in Fig. 9.

4.1 CORRELATION OF STATIC WITH UNSTEADY PRESSURES

From the variation of the static pressure coefficient with free-stream Mach number for an orifice located 0.05 diameter aft of the shoulder (Figs. 10a-d), one may approximate the Mach numbers at which the alternating flow condition is likely to occur. Curves are shown for cones of 15-, 20-, 25-, and 30-deg half angles and various angles of attack (data obtained from Ref. 3). The discontinuities in the curves indicate transition from separated to attached flow conditions on the cylinder. Unsteady pressures result when the flow fluctuates between the separated and attached states. Thus, discontinuities in the curves shown in Fig. 10 indicate the possibility of an alternating flow condition occurring. The Mach number ranges of the alternating flow condition observed during the present test are shown by the small grid for corresponding angles of attack. As previously mentioned, unsteady pressure data identified by positive angles of attack were obtained on the leeward side of the model, and those identified by negative angles of attack were obtained on the windward side of the model.

For the 15-deg half-angle cone at zero angle of attack, no discontinuity is apparent in the static data (Fig. 10a), and correspondingly no pressure fluctuations were measured. However, when the model was pitched above 2-deg angle of attack, alternating flow occurred on the leeward side of the cylinder. The Mach number range for the alternating flow condition agrees with the range of Mach numbers between the separated and attached flow conditions defined by the static data.

Alternating flow separation and attachment occurred on both upper and lower surfaces of the 20-deg cone cylinder for the angle-of-attack range investigated, as shown in Fig. 10b. For angles of attack other than zero, the flow became unsteady at lower Mach numbers for the windward side of the cylinder (negative angles of attack), whereas it was delayed to higher Mach numbers for the leeward side (positive angles of attack).

For the 25-deg half-angle cone, alternating flow separation and attachment occurred on both upper and lower surfaces of the cylinder at zero angle of attack and only on the windward side of the model at angles of attack other than zero. Since the variation of the static pressure coefficient with free-stream Mach number shows a large discontinuity in pressure for the leeward side of the model (positive angles of attack, Fig. 10c), it is concluded that a discontinuity in pressure is not a sufficient condition for the occurrence of the alternating flow phenomenon.

The variation of the pressure coefficient with free-stream Mach number for the 30-deg half-angle cone also shows a large discontinuity in pressure for all angles of attack (Fig. 10d); however, attachment was stable at zero angle of attack and on the leeward side of the cylinder at angles of attack other than zero. For angles of attack greater than 1 deg, alternating flow occurred on the windward side of the cylinder.

From the results presented in Fig. 10, increasing the cone angle causes the alternating flow condition to occur at higher Mach numbers. The effect of angle of attack on the alternating flow condition is similar to the effect of cone angle. The leeward side of the cylinder at angle of attack showed the effect of increasing cone angle, whereas the windward side of the cylinder showed the effect of decreasing cone angle. The alternating flow conditions may occur at angles of attack other than zero, even though they do not occur at zero angle of attack. (Examples are the 15- and 30-deg half-angle cone cylinders.)

The magnitude of the pressure fluctuations measured for alternating flow conditions is obviously related to the difference between the static pressures at separation and at attachment. Comparisons of the axial pressure distributions at Mach numbers immediately below and above the range of the alternating flow conditions are shown in Fig. 11 for the 15-, 20-, 25-, and 30-deg cone cylinders. The differences between the static pressure coefficients from Fig. 11 are presented in Fig. 12. The values of unsteady peak-to-peak pressure coefficients measured for alternating flow conditions are also presented in Fig. 12 for comparison. The unsteady pressure data were taken from the oscillograph records. The

sign convention used to determine these ΔC_p values was to reference all changes in pressure to the attached flow pressures. In general, these figures show good agreement between predicted values of ΔC_p taken from static data and the measured unsteady pressure coefficients. Although the maximum measured unsteady pressure coefficient was approximately 0.43 at $x/D = 0.10$ (Fig. 12c), the static data indicate that the maximum value may be as large as 0.60 at $x/D = 0.05$.

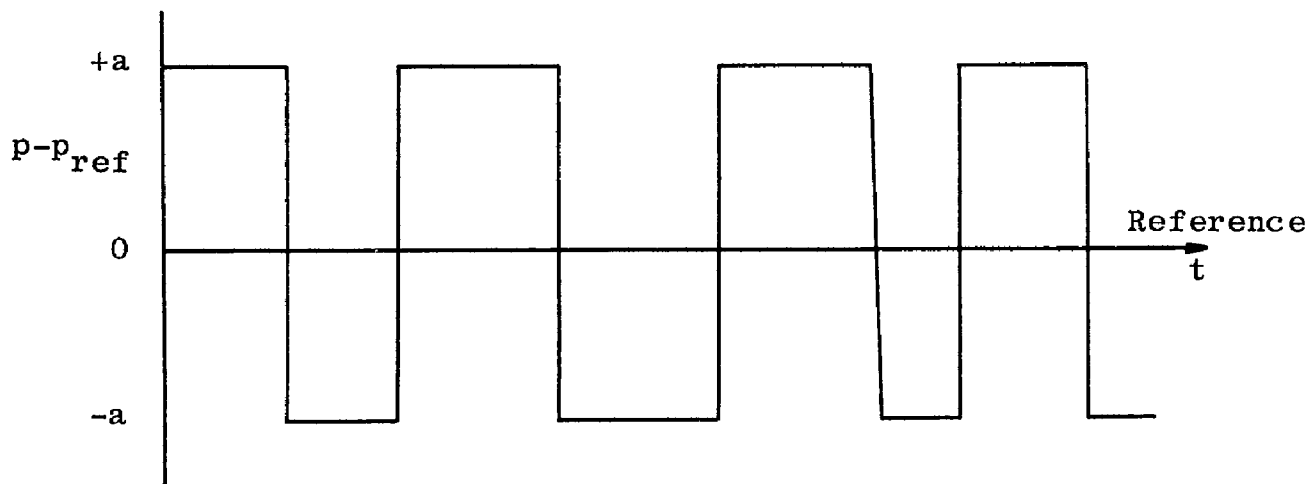
At the location of the shock wave, Fig. 12 shows that the fluctuations decrease to zero, and downstream of this point, the load produced by the pressure fluctuations changes direction.* This change in load direction will result in a large time-varying couple on a missile skin aft of the cone-cylinder juncture.

4.2 POWER SPECTRUM AND FREQUENCY CHARACTERISTICS

The alternating flow condition is a stationary random process and produces a near rectangular wave form. From a statistical analysis of the random rectangular wave given in Ref. 6, the equation of the power spectrum is:

$$2\pi F(\omega) = \frac{2 \left(\frac{a^2 \mu}{\pi^2} \right)}{\frac{\mu^2}{\pi^2} + f^2} \quad (1)$$

where a is the amplitude of the pressure fluctuation as shown in the following sketch, and μ is the number of sign changes of $(p - p_{ref})$ per second.



*Although no pressure fluctuations existed at the location of the shock wave as a result of the alternating flow, pressure fluctuations existed during the attachment portion of the cycle as a result of the unsteadiness of the shock wave at this location. These shock wave pressure fluctuations have different characteristics, and the peak-to-peak values are not included in Fig. 12 but will be presented in detail in a subsequent report.

For most of the oscillograph records, the values of a and μ were easily determined, and the power spectral density could be approximated by Eq. (1). However, for some conditions where the alternating flow phenomenon had a high frequency of occurrence or was inadequately defined, the values of μ could not be determined with reasonable accuracy. An example of this is shown in Fig. 13a for the 20-deg cone at zero angle of attack and $x/D = 0.10$. For these cases an approximation of the power spectral density could not be made, although the peak-to-peak pressure fluctuations (2a) were defined.

Values of a and μ were determined from selected oscillograph records, and the power spectral density versus frequency was calculated using Eq. (1). Comparison of the calculated power spectrums with ones obtained using the wave analyzer are shown in Figs. 13b-e. Samples of corresponding oscillograph records are also shown in Fig. 13. These power spectrums show that the energy distribution with frequency agrees approximately with the energy distribution obtained from the analysis of a random rectangular wave form. For all alternating flow conditions the largest concentration of power was at the low frequency end of the spectrum.

The rms level of an unsteady pressure having a rectangular wave form is equal to the amplitude of the pressure fluctuation (a). Two methods were used to determine the rms level of the pressure fluctuations, and the results were compared with values of a . First, readings were obtained from an rms voltmeter, and the results did not equal the amplitude of the pressure fluctuation. This lack of agreement may be credited to the lower frequency limit of the voltmeter which was 15 cps. For most of the data, μ was less than 15 per second and the voltmeter apparently failed to analyze the alternating flow output. Second, the rms level was determined by integration of the power spectral densities. These results were approximately equal to corresponding values of a for data having well-defined rectangular wave forms (see Figs. 13b-c).

4.3 COMMENTS ON ALTERNATING FLOW SEPARATION AND ATTACHMENT

The explanation of the alternating flow on a cone cylinder is similar to the explanation given an oscillatory flow attachment on an airfoil in Ref. 7. To have stable attachment both inviscid and viscous requirements of the flow field near the shoulder must be satisfied. The attachment of the flow begins when the momentum of the flow aft of the shoulder directed toward the cylinder is sufficient to support attachment. The momentum component directed toward the surface is indicated by the overexpansion in this region. This attachment results in a large increase in local Mach

number at the shoulder (approximately 2.0 for the cone angles tested) and a corresponding large adverse pressure gradient to decelerate the flow back to free-stream conditions ($M_\infty < 1.0$). As shown in Ref. 3 the boundary layer cannot withstand this gradient and separates at some distance downstream of the shoulder. This local separation being in a supersonic flow field produces a near normal shock wave, and the accompanying large back pressure feeds forward to the shoulder. The resulting forward progression of the separation point can cause the flow to revert to the initial separated flow conditions. With the original conditions established the cycle starts again with attachment. This type of flow field represents an alternating unbalance between the large pressure rise through the shock that exceeds the values required to separate the flow and the small pressure rise that is too small to maintain fully separated conditions.

4.4 SCALE EFFECTS

As pointed out in Refs. 2 and 3, two known scale effects do exist. One is that the Mach number at which the alternating flow condition occurs decreases with increasing model size. The other is that the value of ΔC_p varies with model size. As shown in Ref. 3, these effects can only be approximated by adding a boundary trip to the small models.

From Eq. (1) a change in μ would result in a change in the level of the power spectrum. Also a change in μ would result in a different distribution of the power $2\pi F(\omega)$ with frequency. Although no data are available on the effect of scale or Reynolds number on μ , it is likely that an effect does exist.

4.5 DISCUSSION

The principal result of this investigation has been to show the importance of static pressure measurements and the correlation of these measurements with the unsteady pressures. From static pressure distributions, one may determine the regions of the model to be subjected to unsteady loads, the free-stream Mach number at which this will occur, and the peak-to-peak and rms amplitude of these loads. Also, with a limited amount of dynamic measuring devices, such as one transducer or motion picture schlieren (used to evaluate μ) and static results (used to evaluate ΔC_p), one can approximate the power spectrum of the pressure fluctuations at any point on the body surface.

One of the important remaining unknowns is the problem of scale and Reynolds number effect. Thus, for future investigations, an effort should be made to test larger scale models. However, for the present it is interesting to note that this type of unsteady pressure, in general, produces considerable power at the low frequencies, down to near 1 cps. Most large missiles have low frequency resonant characteristics that could couple with the pressure fluctuations.

5.0 CONCLUSIONS

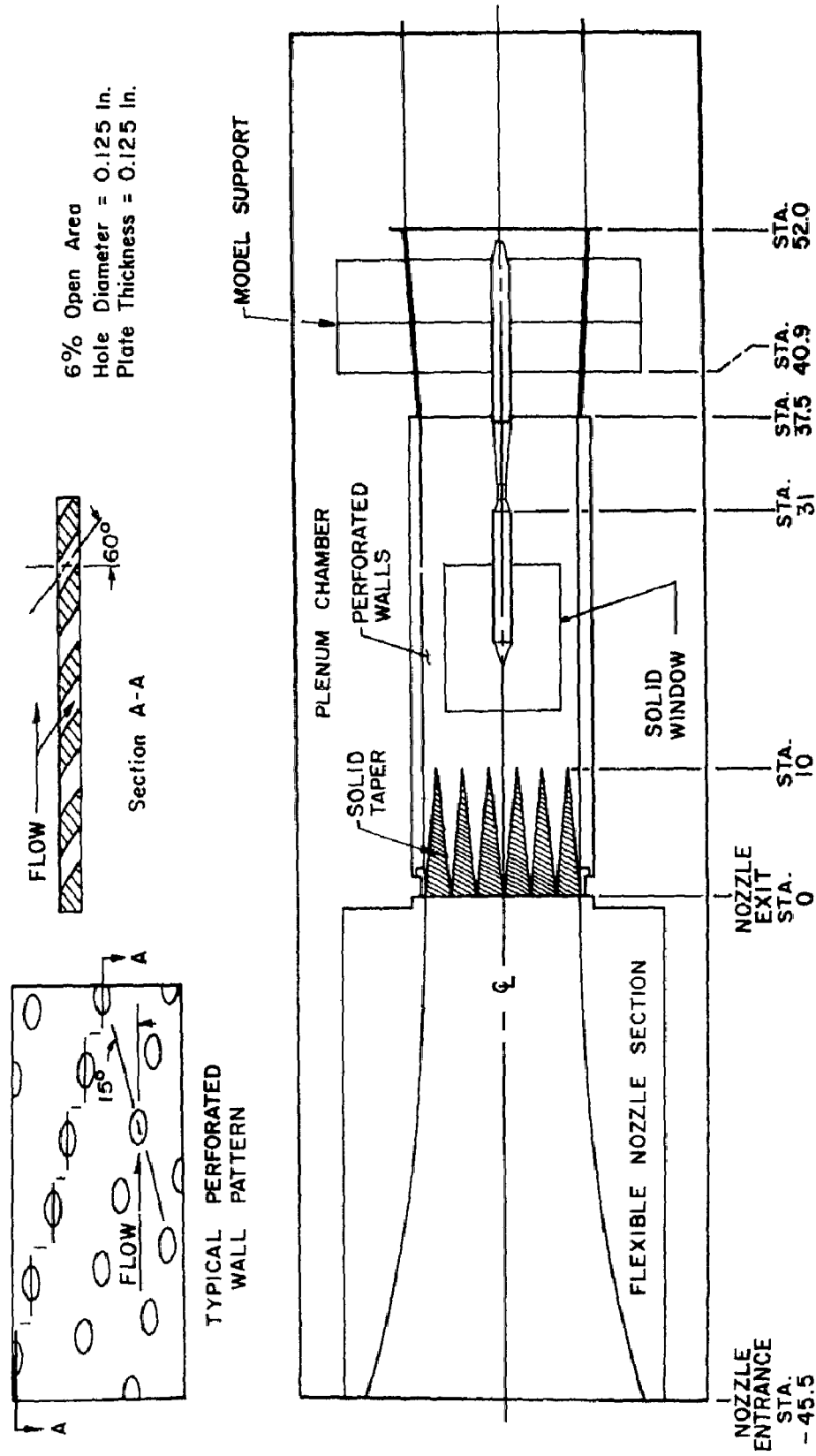
A survey of the static and unsteady pressure measurements for the alternating separated and attached flow on cone-cylinder bodies results in the following conclusions:

1. From static pressure distributions one may determine regions of the model to be subjected to unsteady loads, the free-stream Mach number at which this will occur, and the peak-to-peak and rms amplitude of these loads.
2. The unsteady peak-to-peak pressures are approximately equal to the difference between the static pressures on the cylindrical surface at separation and attachment.
3. The energy distribution with frequency agrees approximately with the statistical analysis of a random rectangular wave form.
4. Increasing the cone angle causes the alternating flow condition to occur at higher Mach numbers. The effect of angle of attack on the alternating flow condition is similar to the effect of cone angle. The leeward side of the cylinder shows the effect of increasing cone angle, and the windward side of the cylinder shows the effect of decreasing cone angle.
5. The alternating flow condition results in a large concentration of power at the low frequency end of the spectrum.

REFERENCES

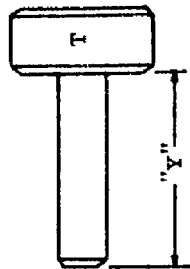
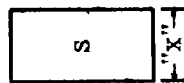
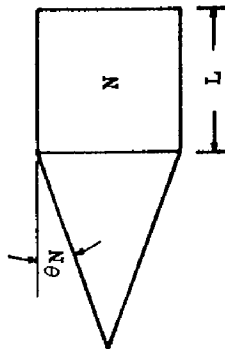
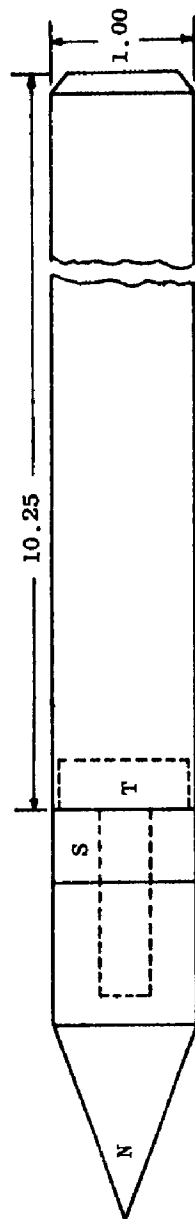
1. Robertson, J. E. "Measurement of the Pressure Fluctuations in the Test Section of the 1-Foot Transonic Tunnel in the Frequency Range from 5 to 1250 cps." AEDC-TDR-62-109, May 1962.

2. Chevalier, H. L. and Robertson, J. E. "Unsteady Pressures and Scale Effects on Models of the Titan B Mark 4 Re-entry Body at Transonic Speeds." AEDC-TDR-62-178, November 1962.
3. Robertson, J. E. and Chevalier, H. L. "Characteristics of Steady-State Pressures on the Cylindrical Portion of Cone-Cylinder Bodies at Transonic Speeds." AEDC-TDR-63-104, August 1963.
4. Test Facilities Handbook, (5th Edition). "Propulsion Wind Tunnel Facility, Vol. 3." Arnold Engineering Development Center, July 1963.
5. Austin, R. F. and Trail, G. C. Jr. "The Design and Dynamic Calibration of a Pressure Transducer System for Unsteady Pressure Measurements." AEDC-TDR-63-29, March 1963.
6. Schwartz, Mische. Information Transmission Modulation and Noise. McGraw-Hill Book Company, Inc., New York, N. Y., 1959.
7. Lindsey, Walter F. and Landrum, Emma Jean. "Compilation of Information on the Transonic Attachment of Flows at the Leading Edges of Airfoils." NACA TN 4204, February 1958.



TUNNEL STATION IN INCHES

Fig. 1 Test Section of the 1-Foot Transonic Model Tunnel



Nose Cone

	θ_N	L
N ₁	10°	0
N ₂	15°	0
N ₃	20°	0
N ₄	25°	0
N ₅	30°	0
N ₆	15°	1
N ₇	25°	1

Nose Shim

	"X"
S ₁	0.10
S ₂	0.20
S ₃	0.30
S ₄	0.40
S ₅	0.50
S ₆	0.60
S ₇	0.70
S ₈	0.80
S ₉	0.90
S ₁₀	1.00

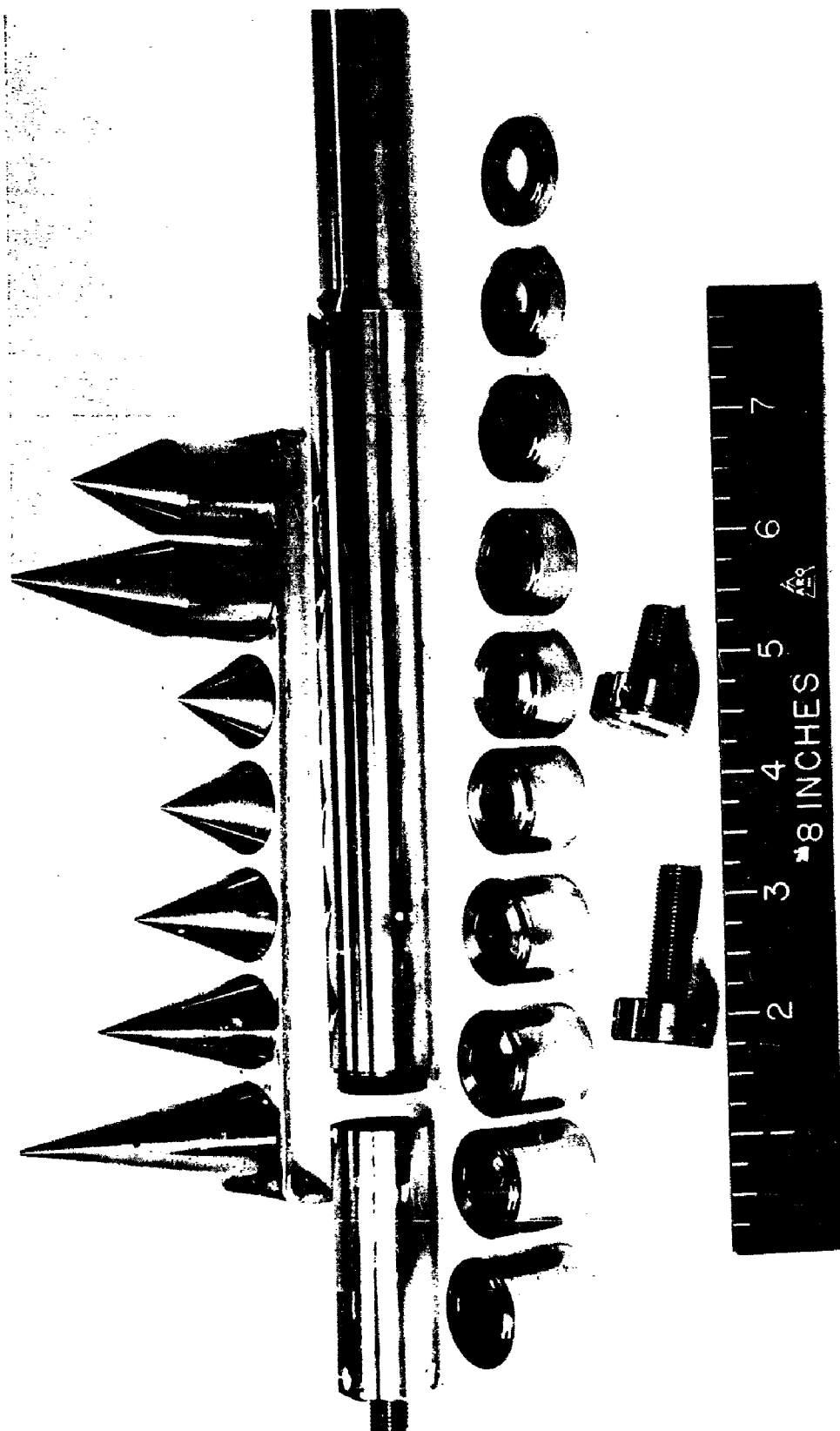
Nose Support

	"Y"
T ₁	0.37
T ₂	0.70
T ₃	1.20

All dimensions in inches.

a. Model Dimensions

Fig. 2 Details of the Cone-Cylinder Model



A E D C
28789-U

b. Photograph of Model Components
Fig. 2 Concluded

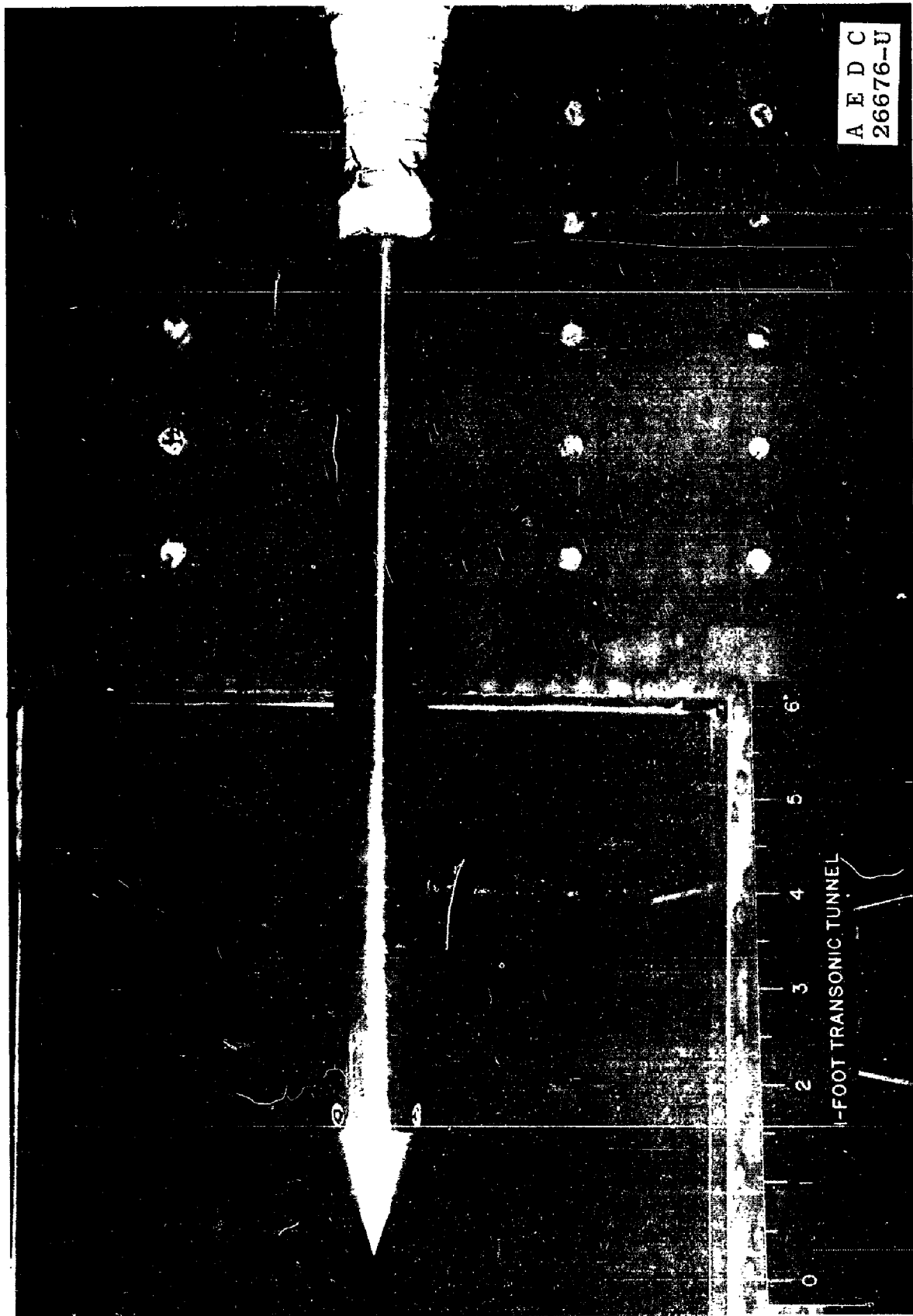
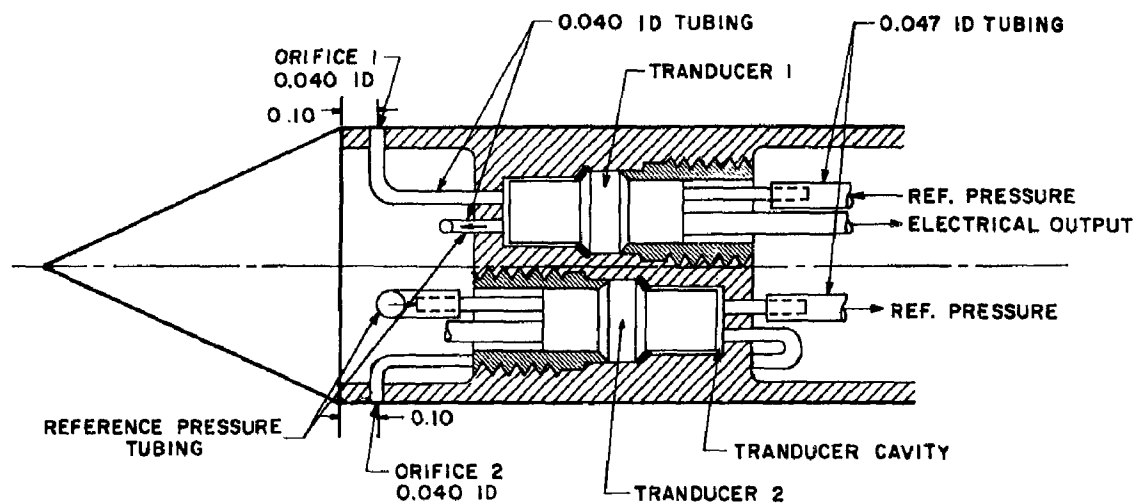
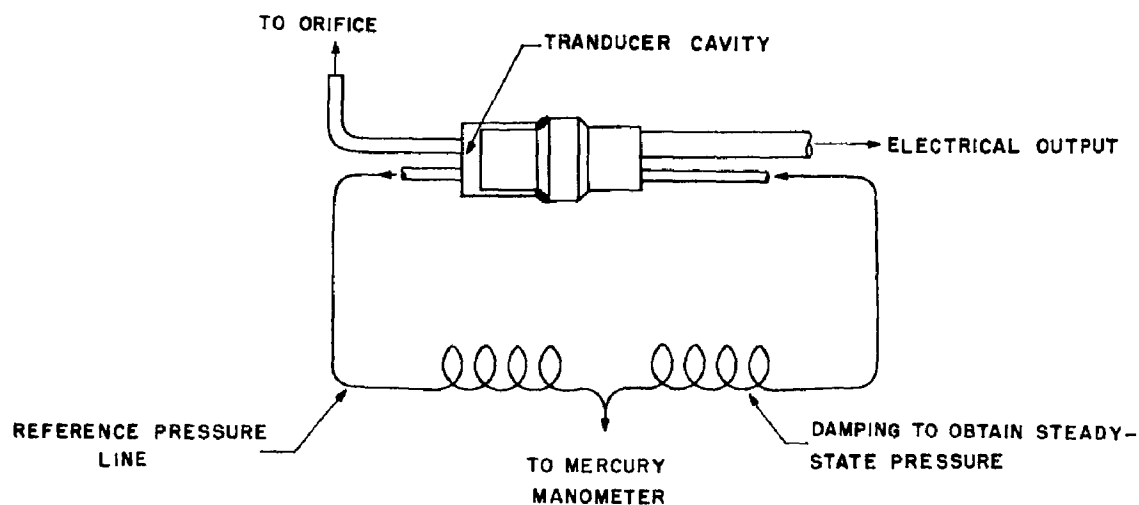


Fig. 3 Model Installation



NOTE: ALL DIMENSIONS IN INCHES

a. Transducer Installations



b. Reference Pressure System

Fig. 4 Details of the Pressure Transducer Mountings

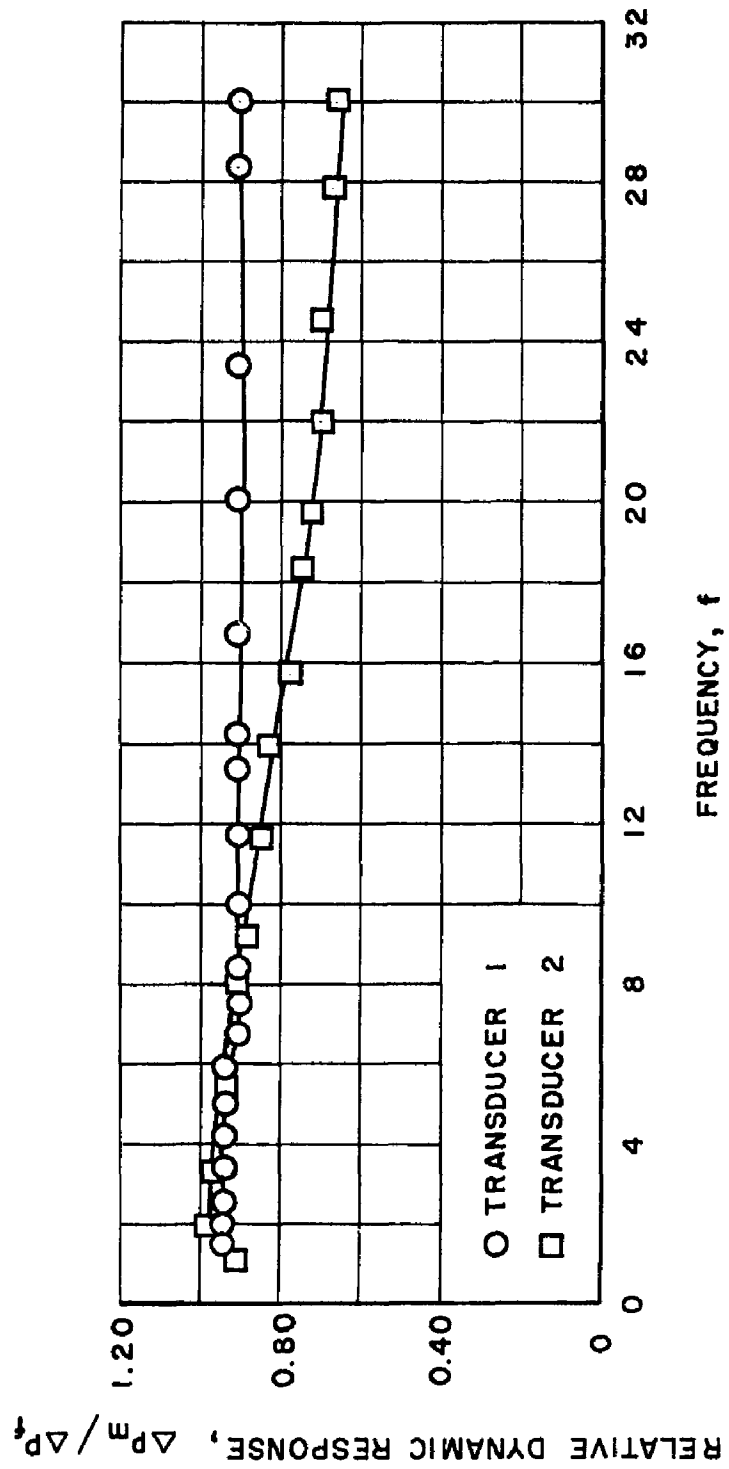


Fig. 5 Dynamic Response of the Model Transducer System Relative to a Flush-Mounted Transducer

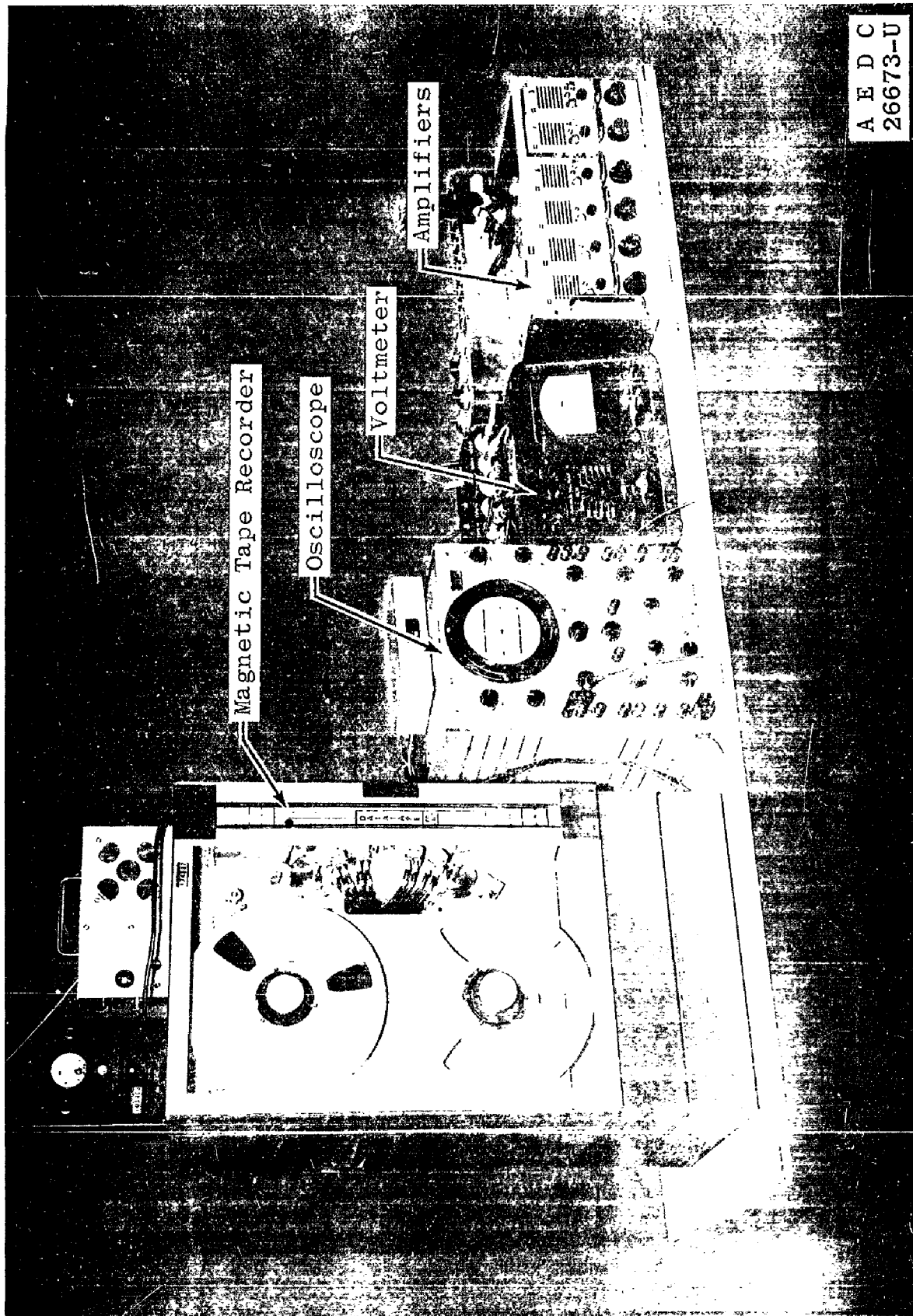


Fig. 6 Instrumentation for Data Recording

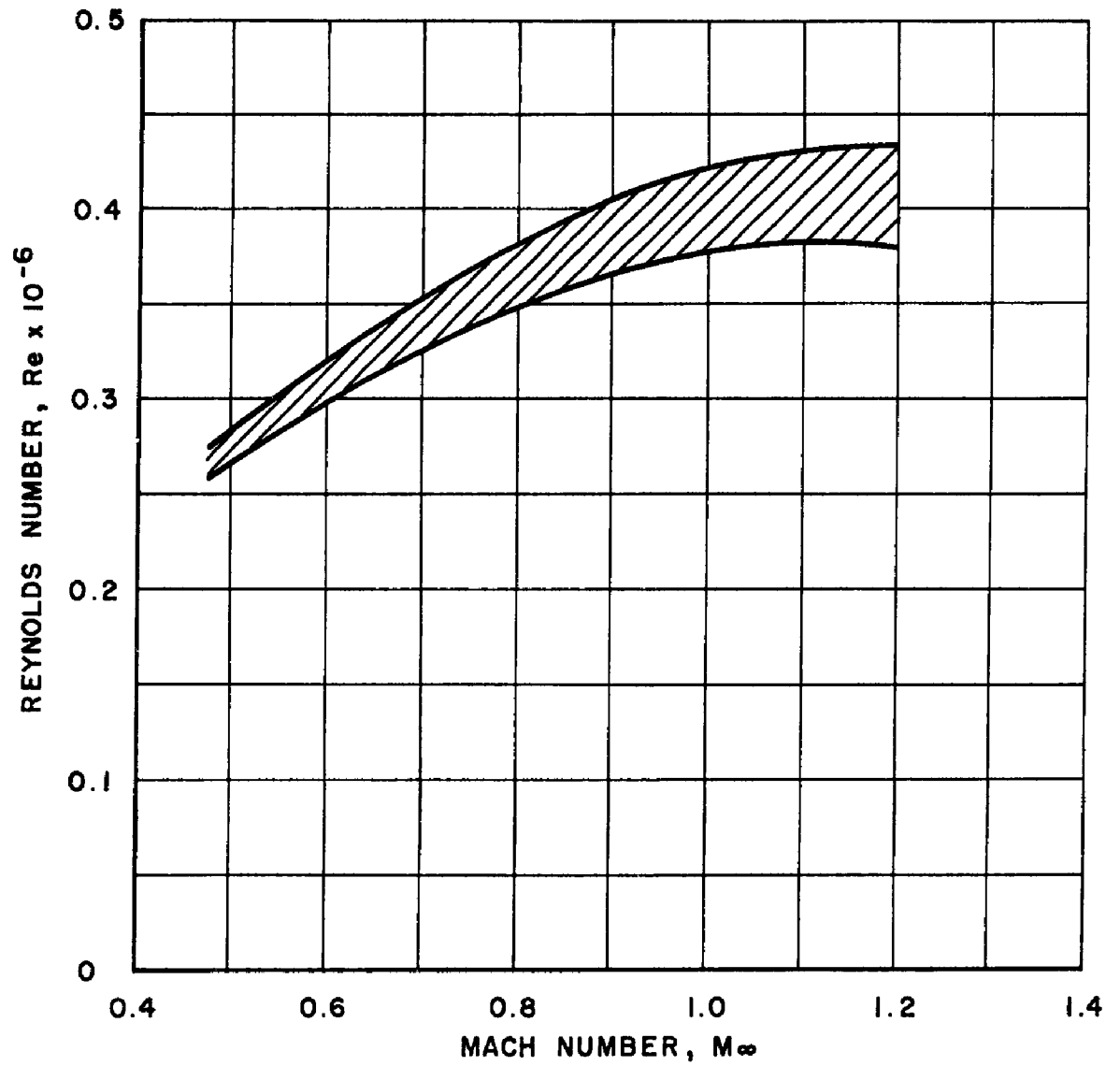


Fig. 7 Variation of Reynolds Number with Mach Number

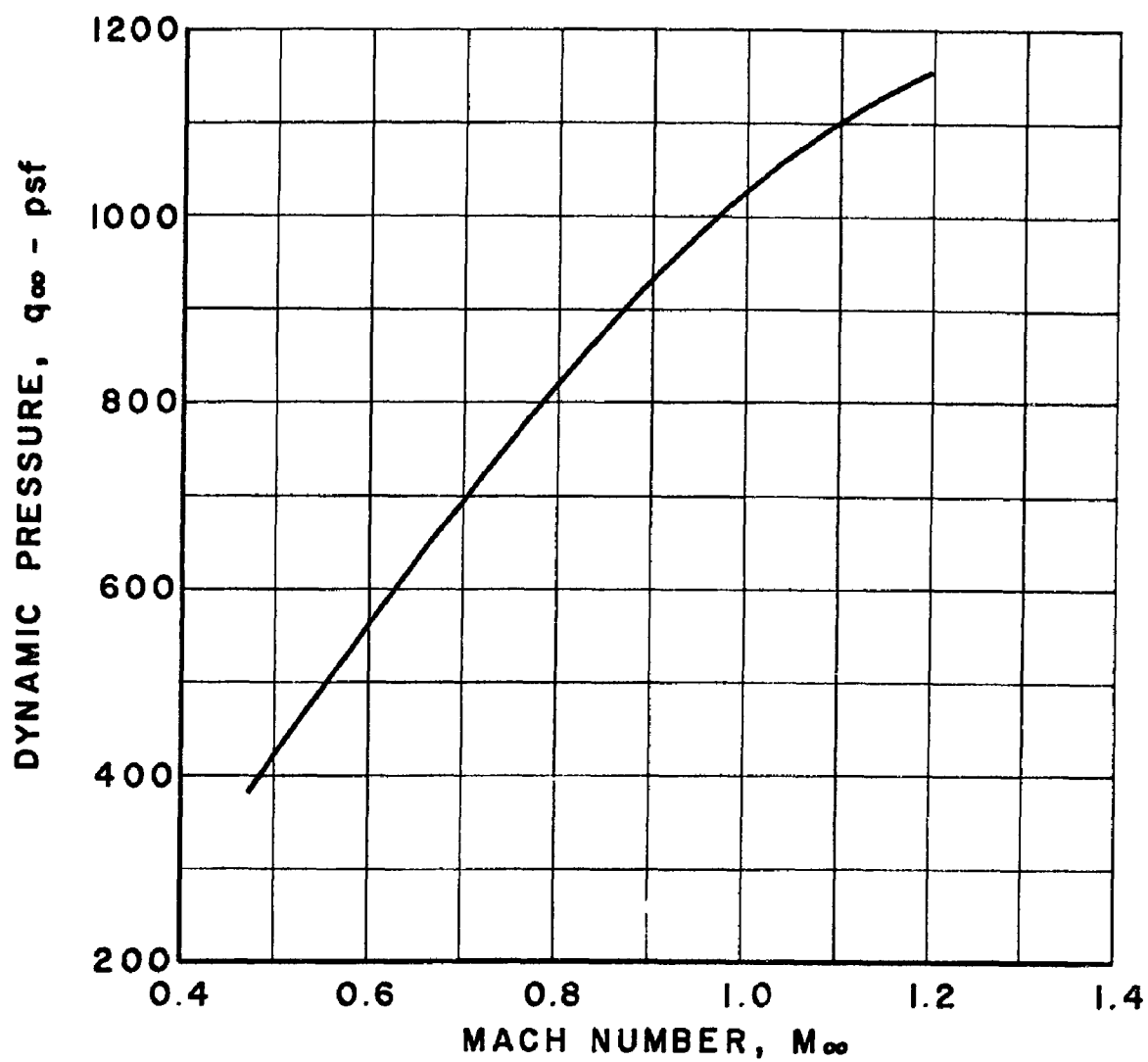


Fig. 8 Variation of Dynamic Pressure with Mach Number



$t = 0$ sec



$t = 15/400$ sec



$t = 5/400$ sec



$t = 20/400$ sec

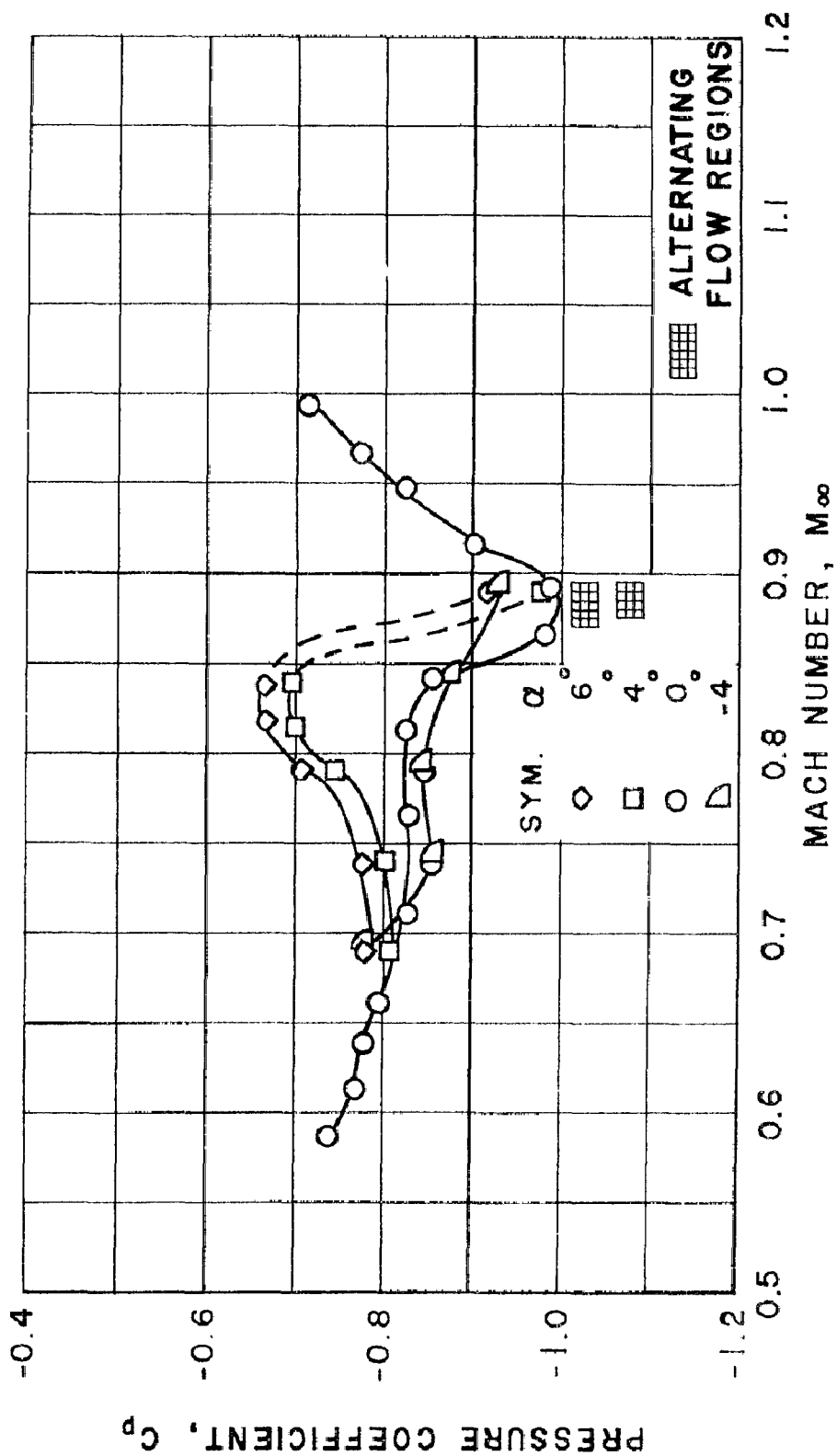


$t = 10/400$ sec



$t = 40/400$ sec

Fig. 9 Typical Time Sequence Photographs of the Alternating Separation and Attachment Flow Conditions at $M_\infty = 0.87$, 20-deg Cone Angle, Taken at 400 frames/sec



$\alpha, \theta_N = 15 \text{ deg}$

Fig. 10 Variation of Pressure Coefficient with Mach Number for Various Angles of Attack α , $x/D = 0.05$

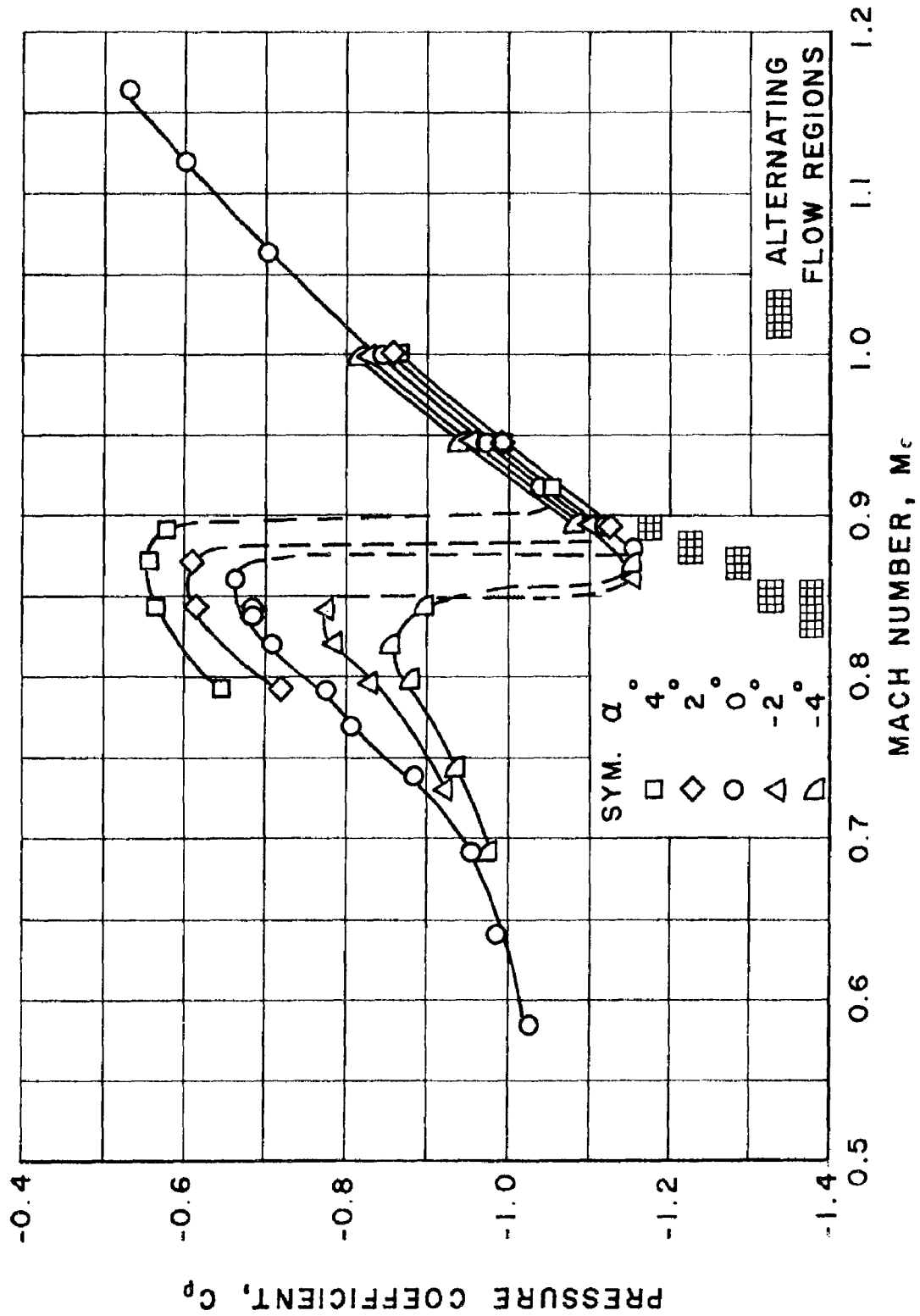
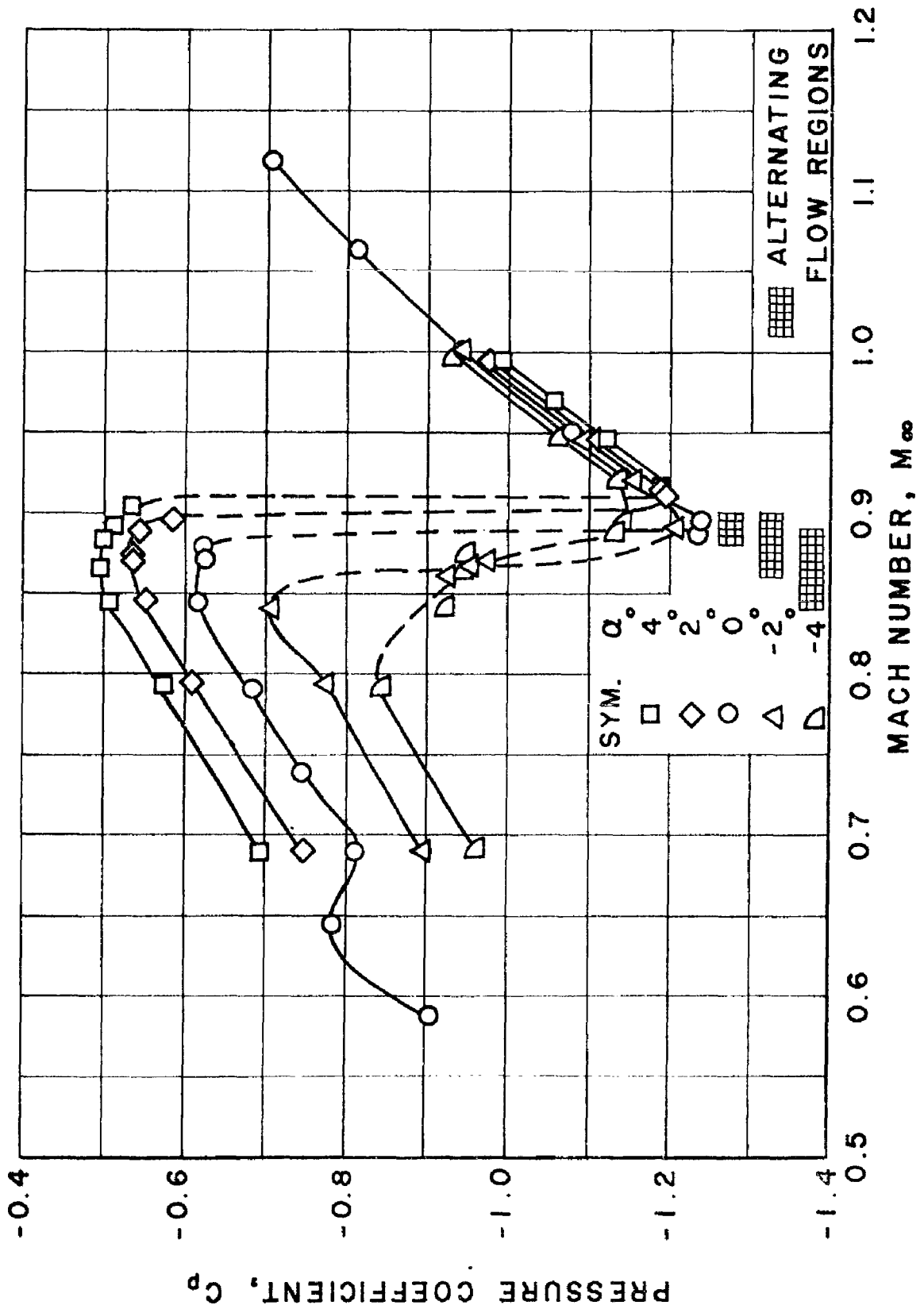
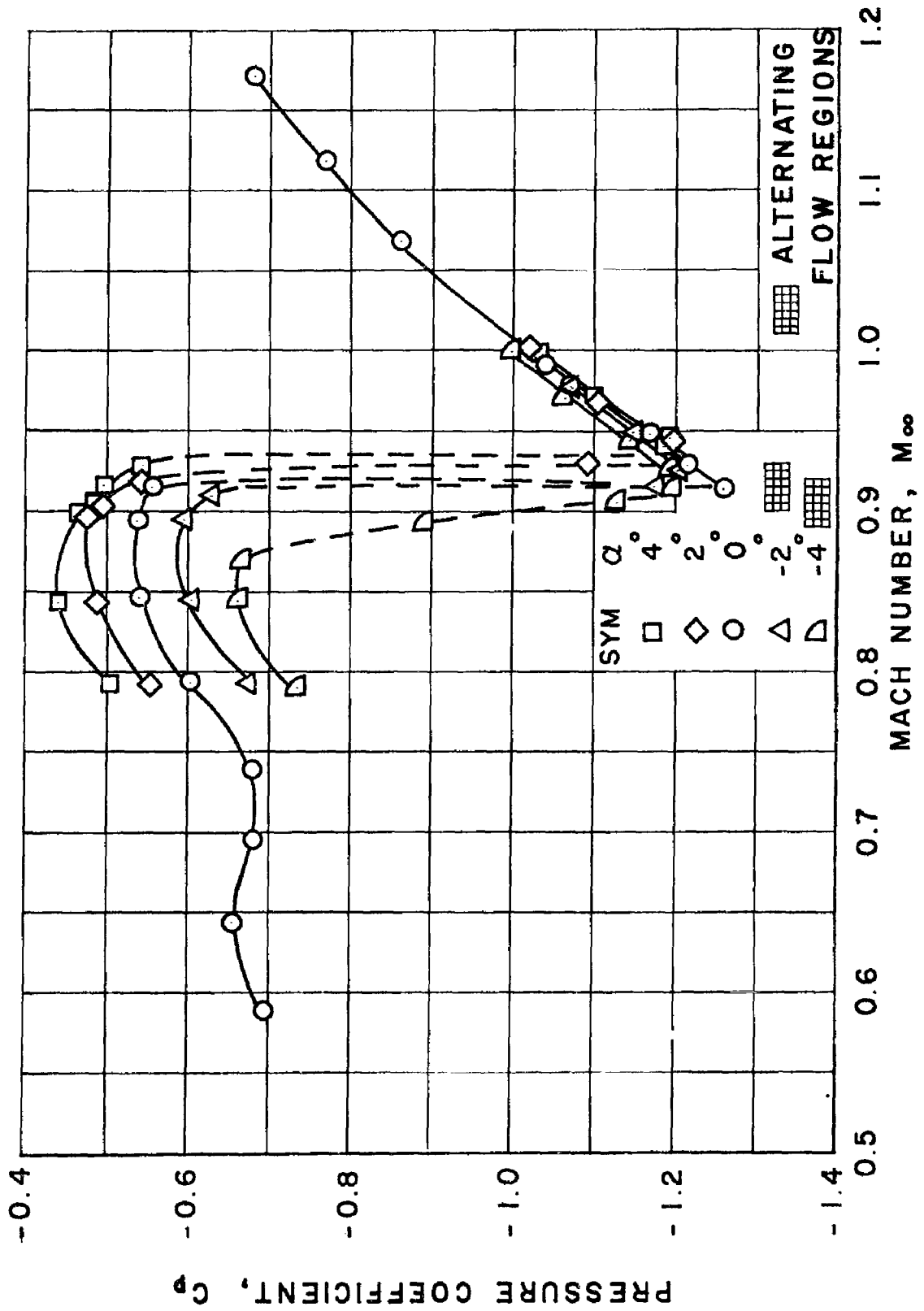
b. $\theta_N = 20^\circ$

Fig. 10 Continued



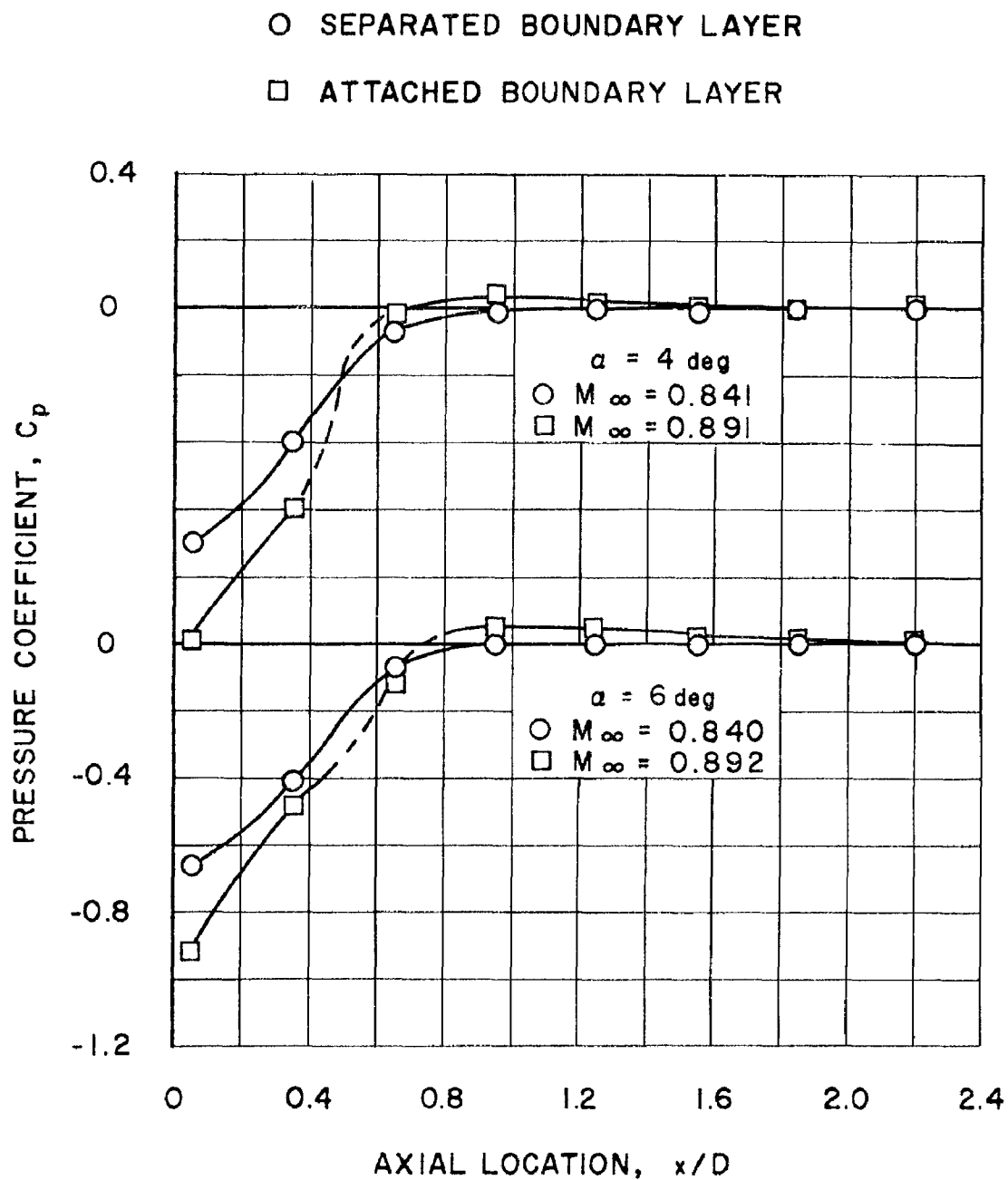
c. $\theta_N = 25^\circ$

Fig. 10 Continued



d. $\theta_N = 30^\circ$

Fig. 10 Concluded



$\alpha = 15$ deg

Fig. 11 Comparison of Pressure Distributions at Mach Numbers above and below the Mach Number Range of the Alternating Flow

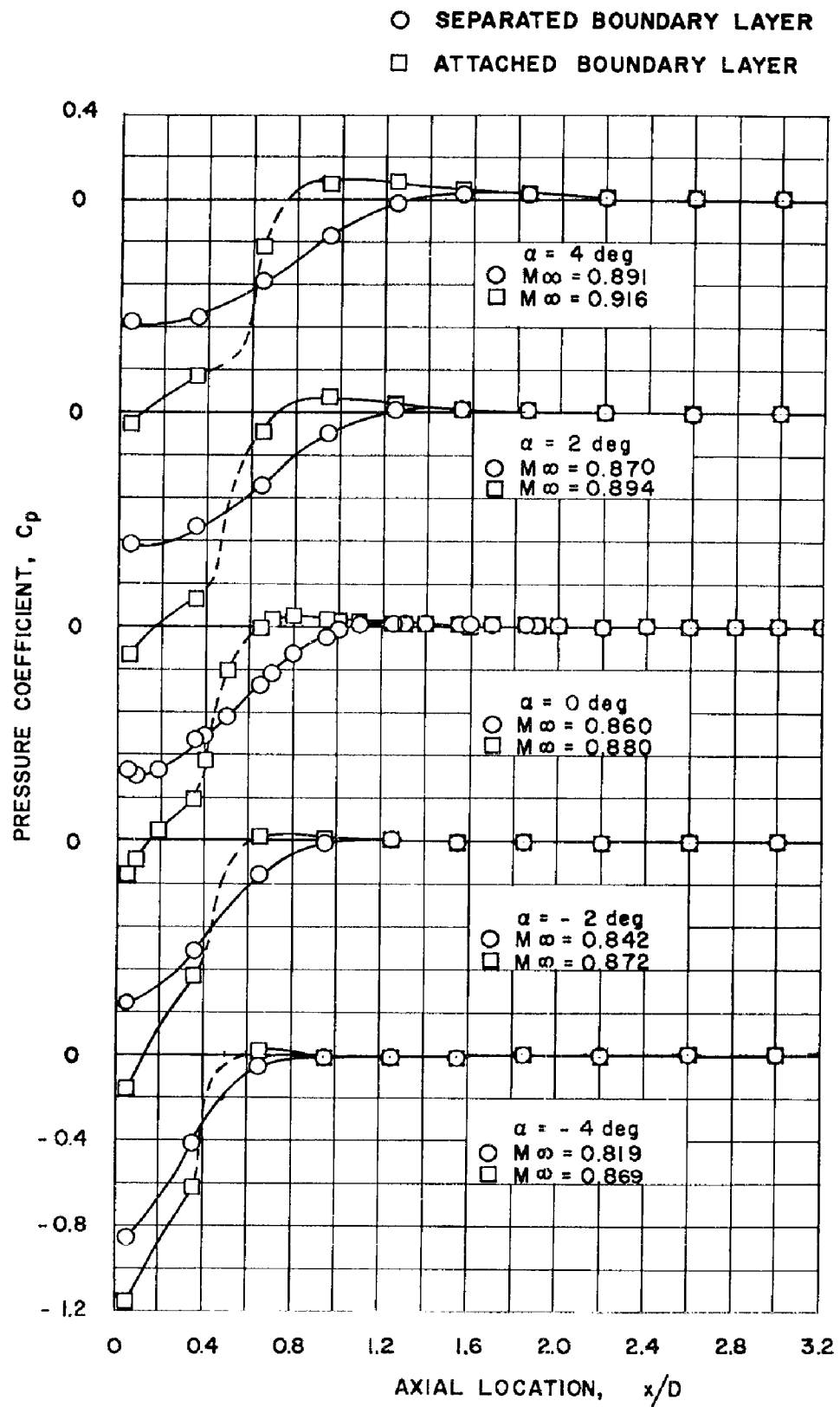
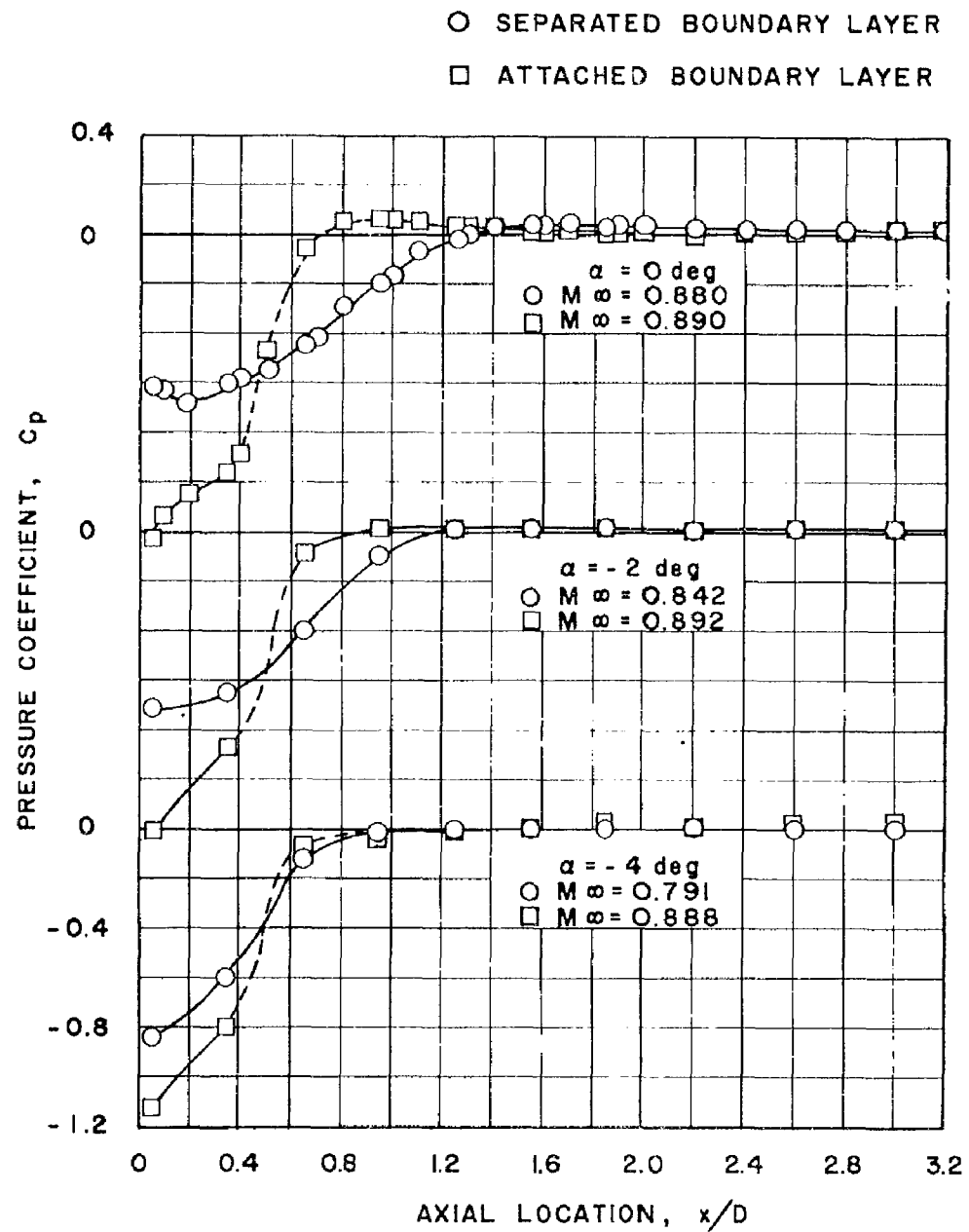
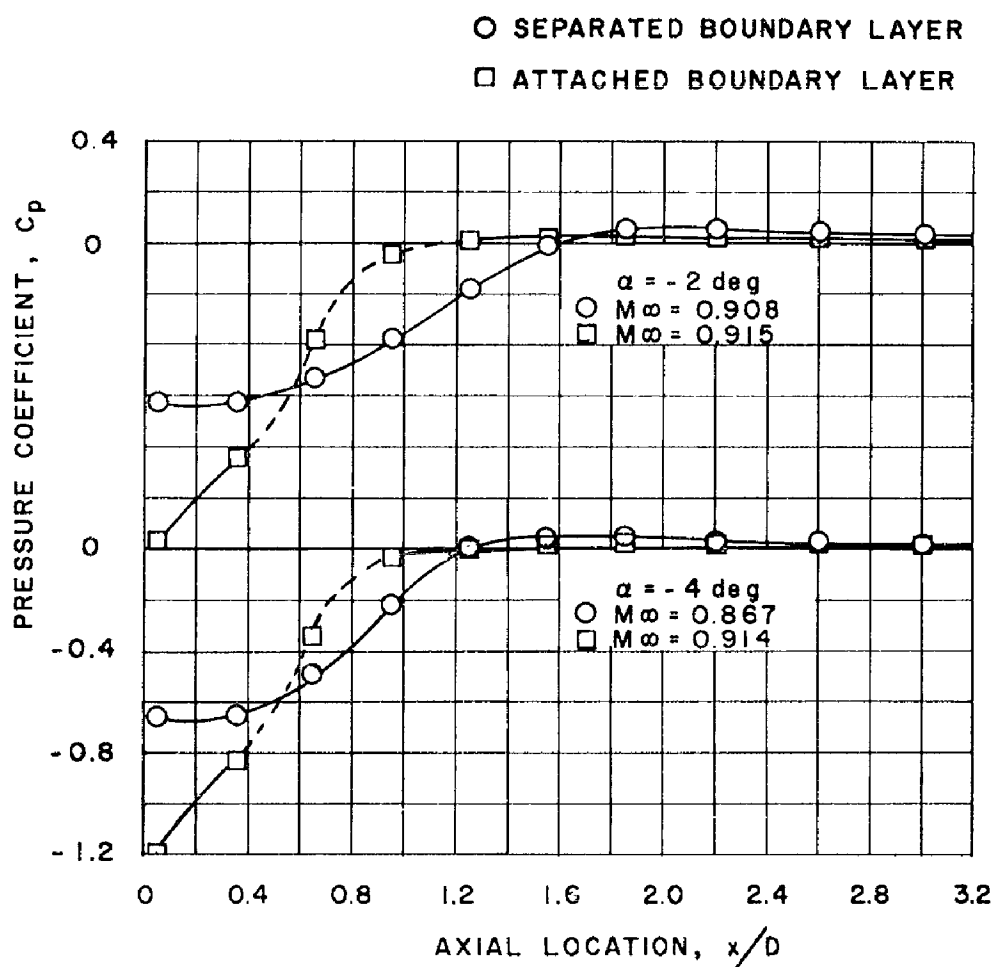
b. $\theta_N = 20 \text{ deg}$

Fig. 11 Continued



c. $\theta_N = 25 \text{ deg}$

Fig. 11 Continued



d $\theta_N = 30 \text{ deg}$

Fig. 11 Concluded

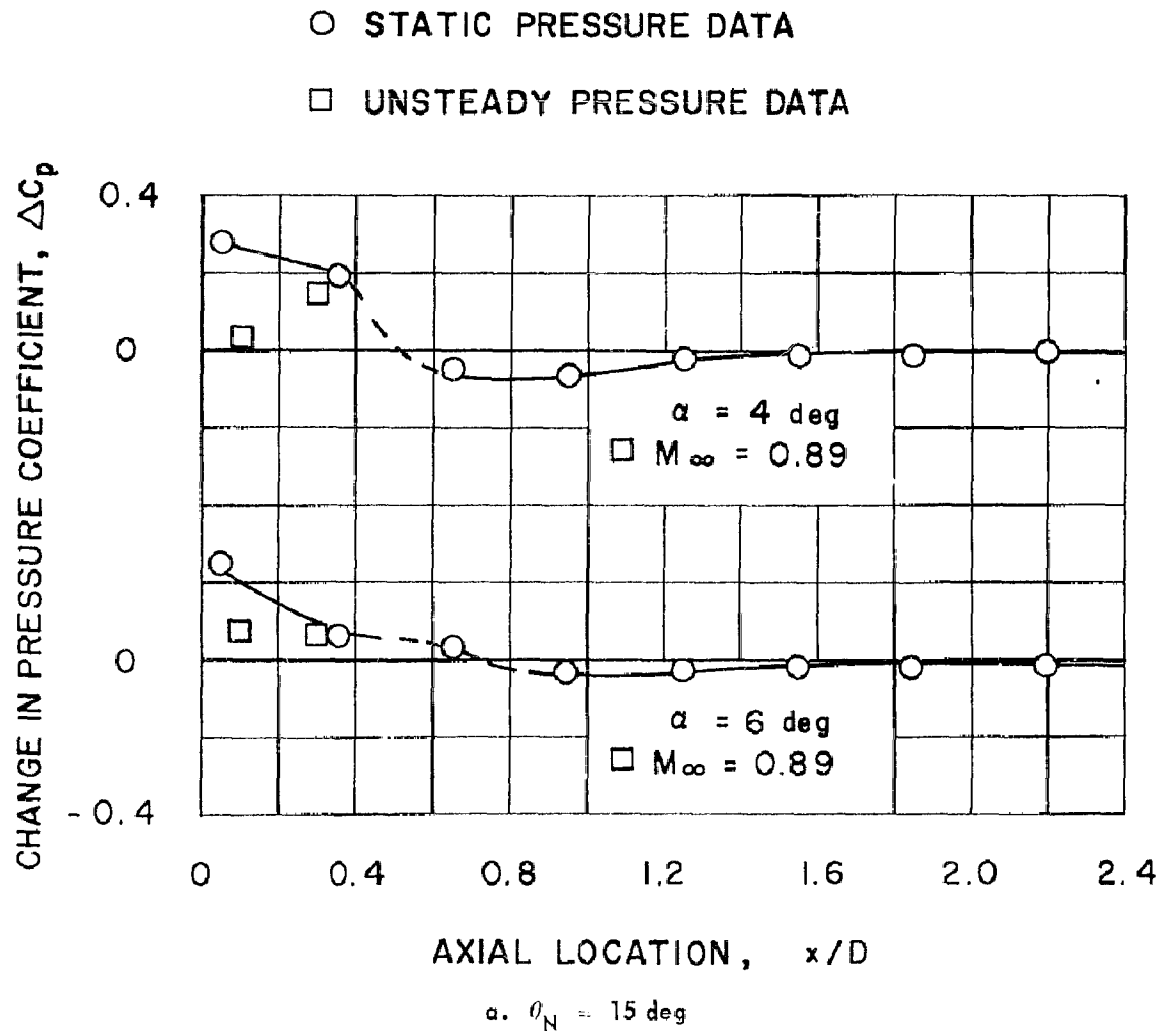


Fig. 12 Comparison of Static Peak-to-Peak Pressure Coefficients with Unsteady Peak-to-Peak Pressure Coefficients

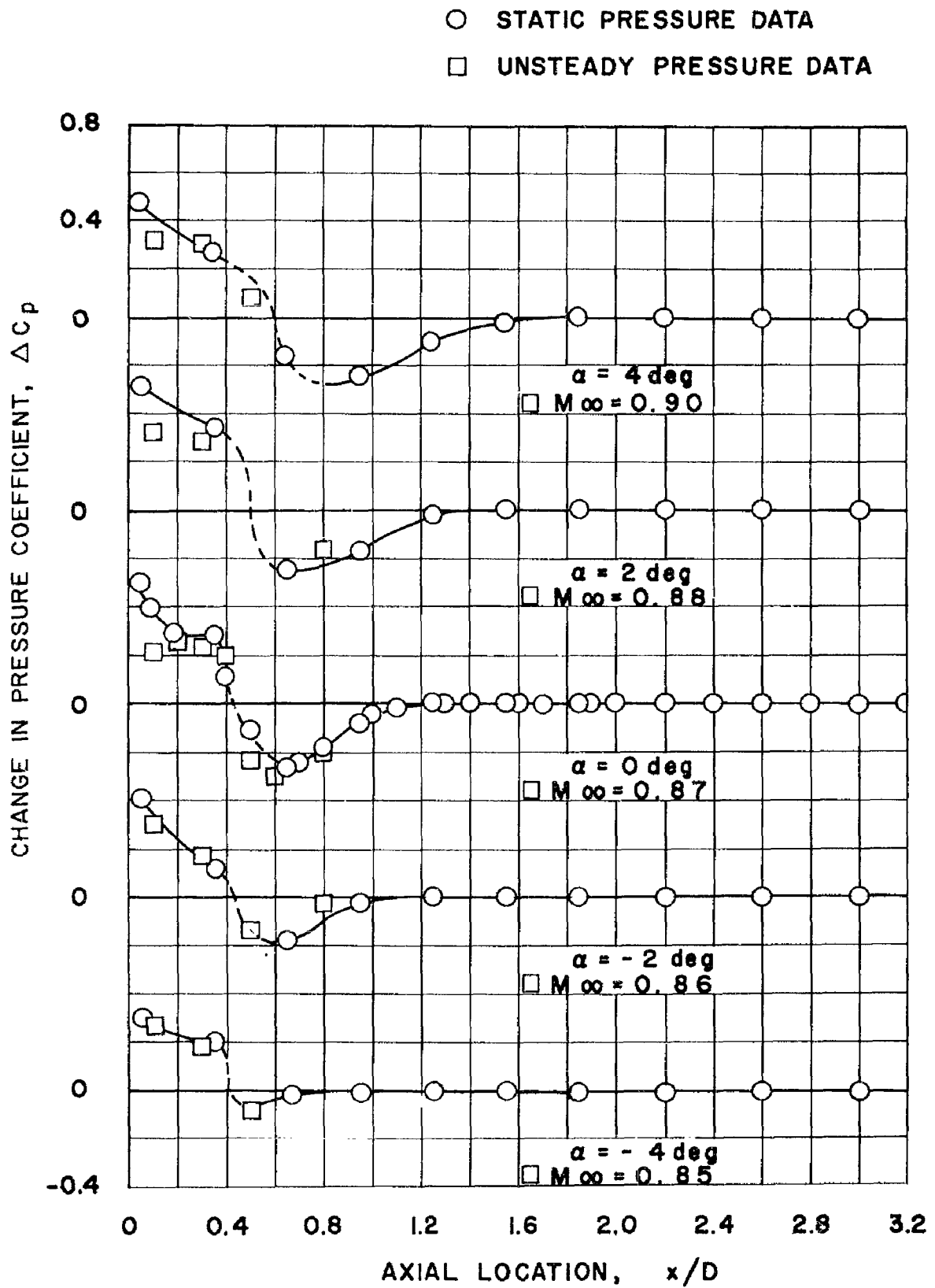
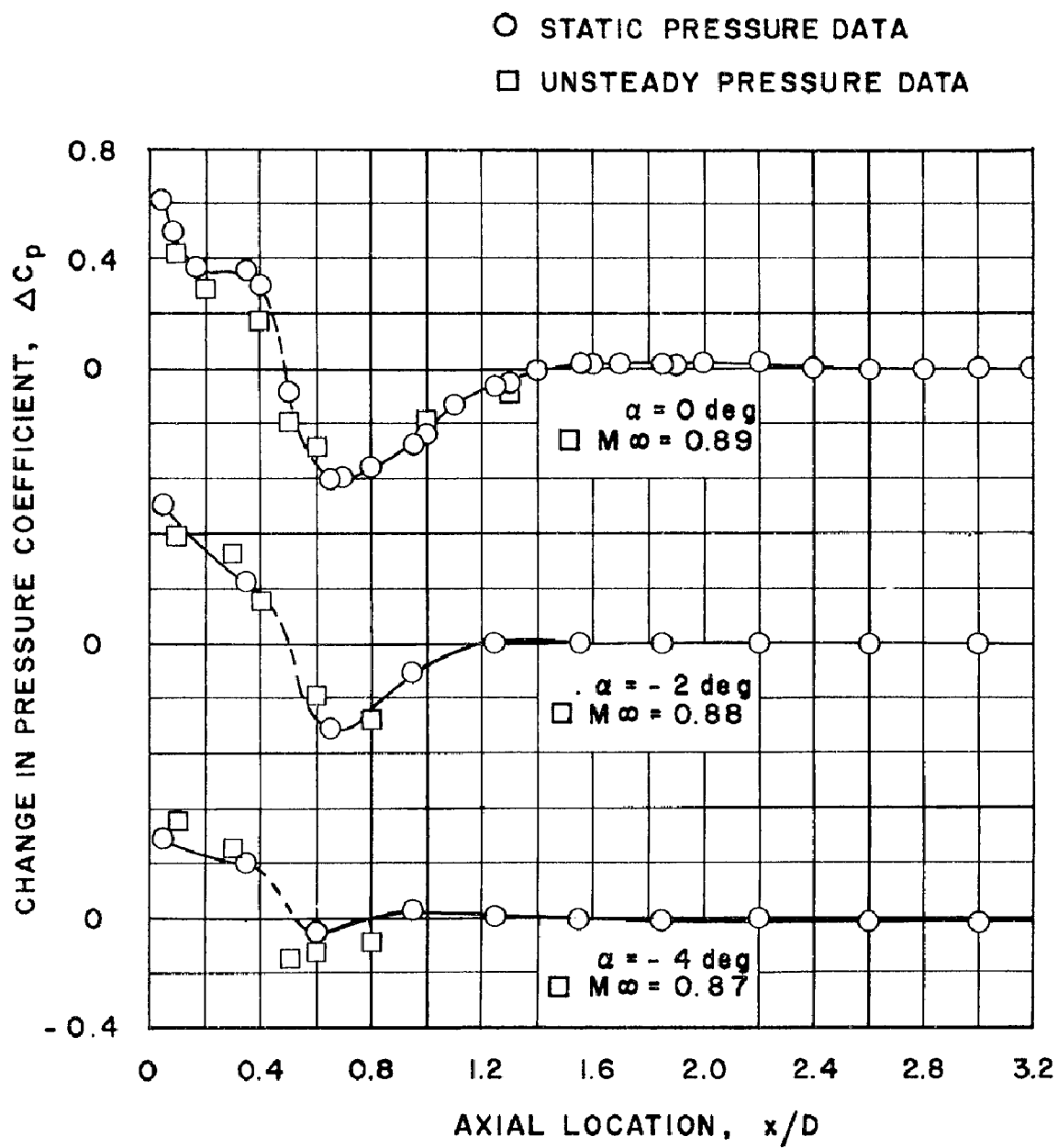
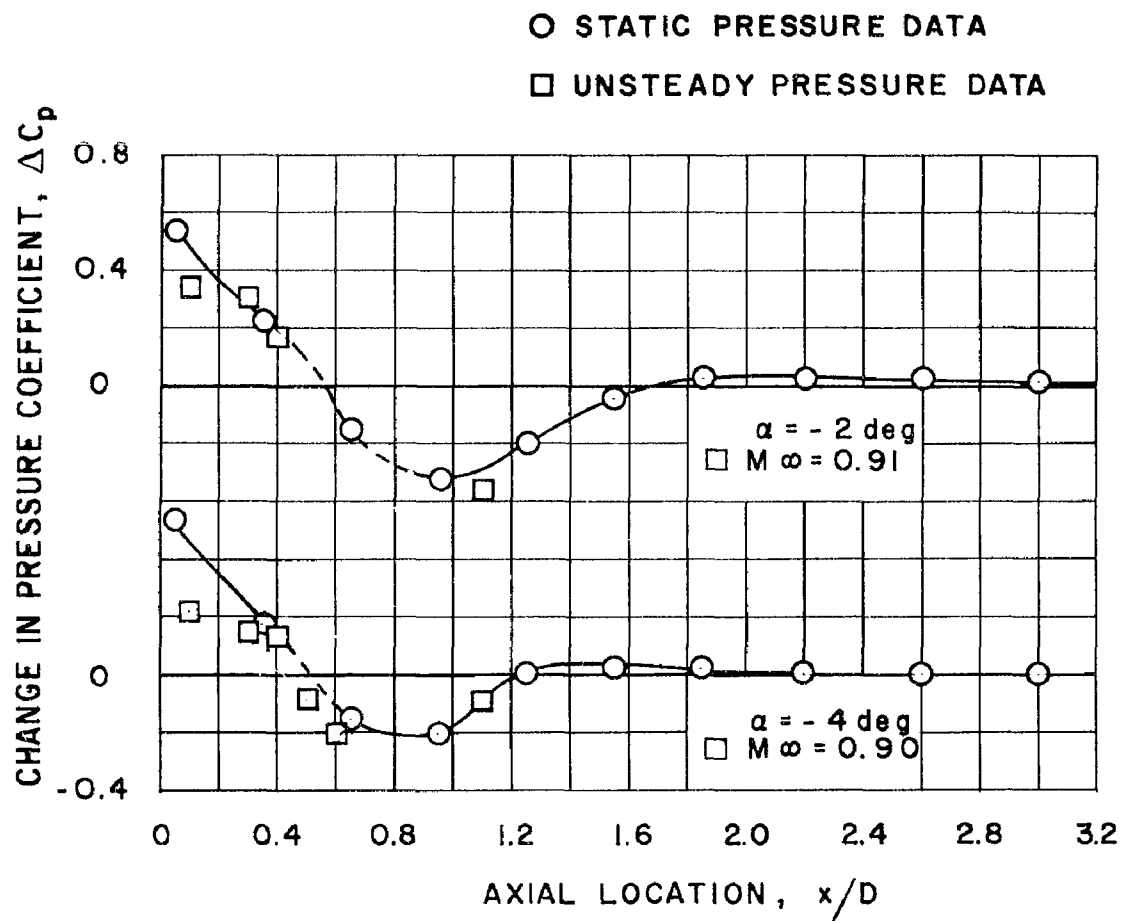
b. $\theta_N = 20 \text{ deg}$

Fig. 12 Continued



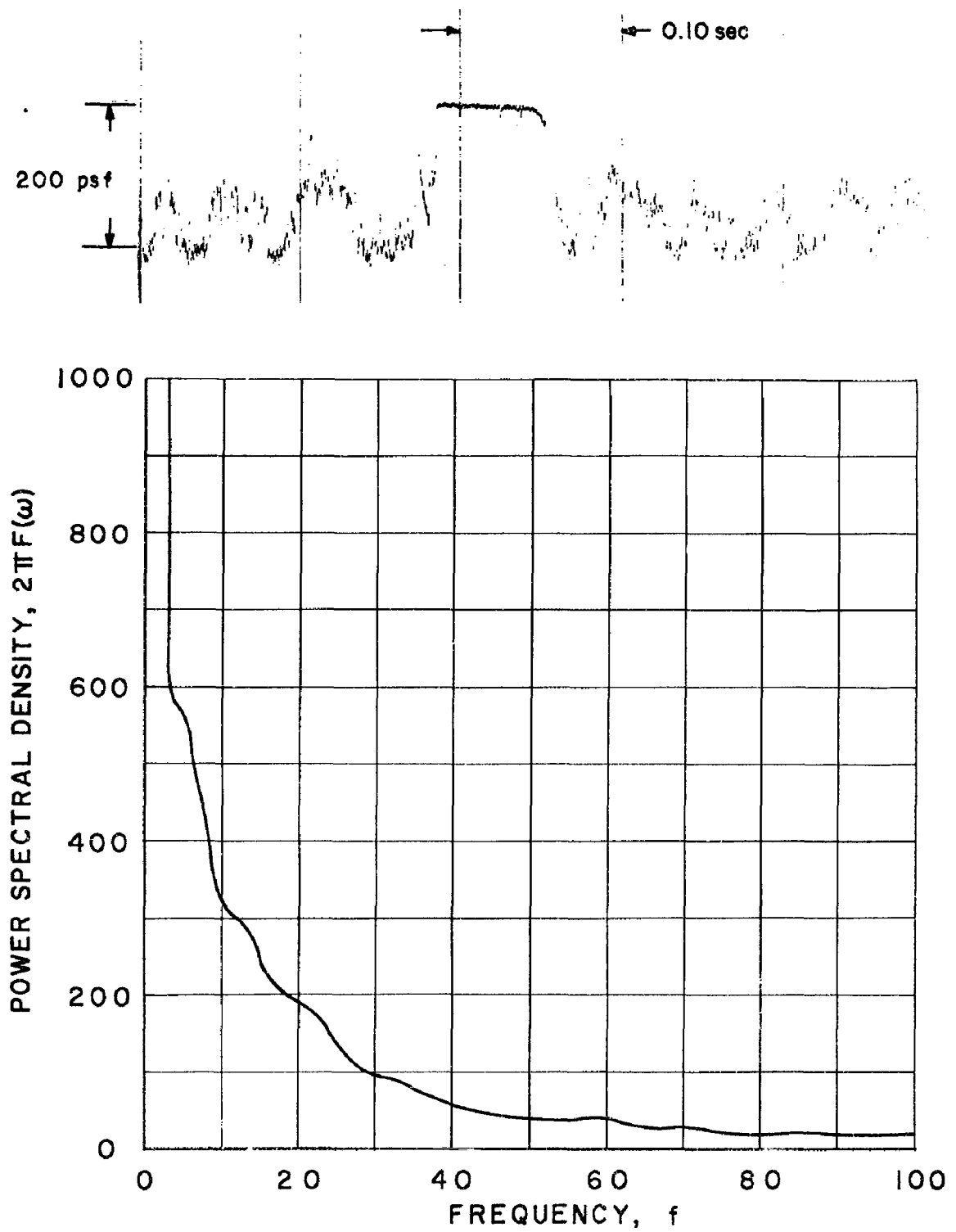
c. $\theta_N = 25 \text{ deg}$

Fig. 12 Continued

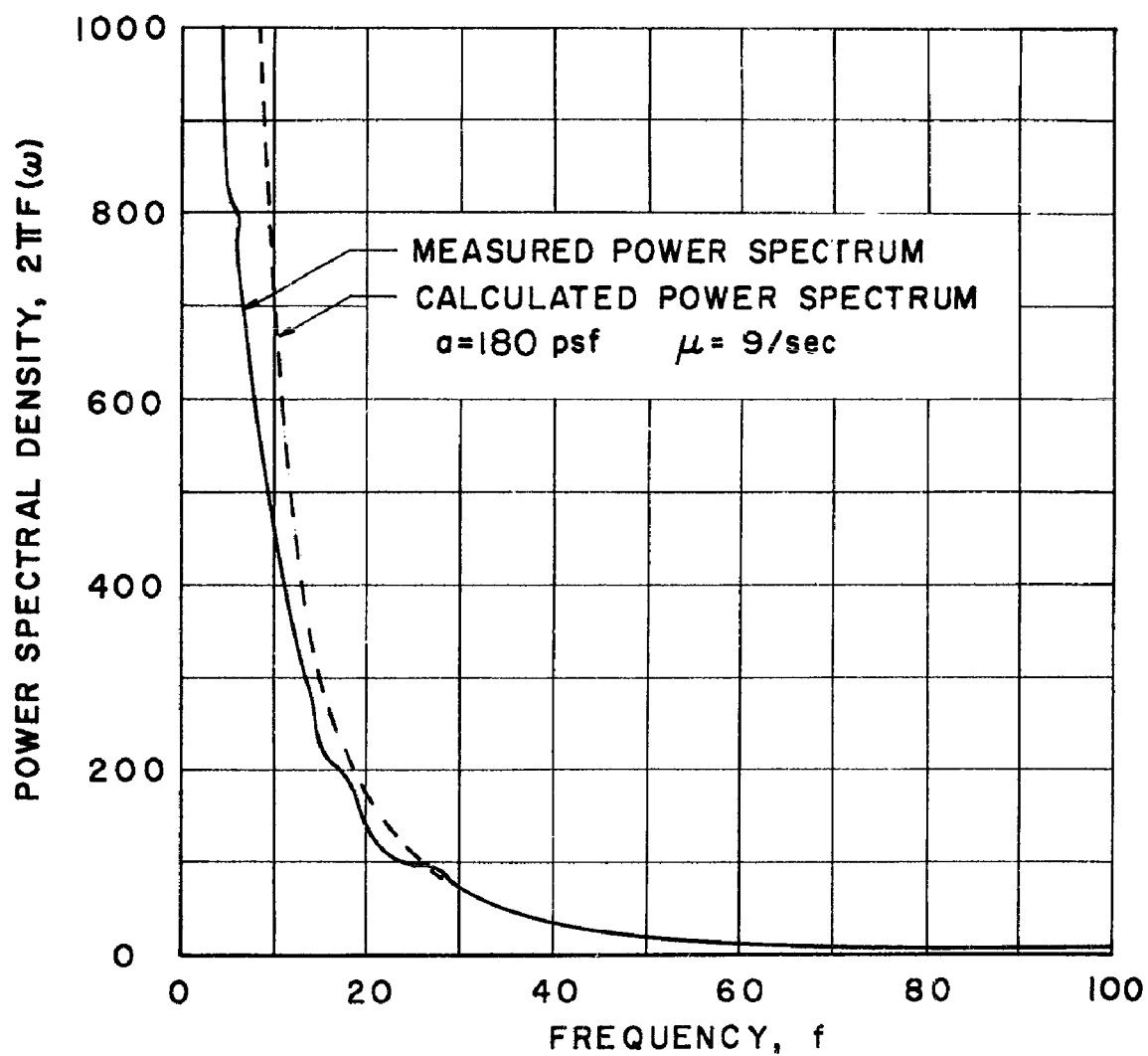
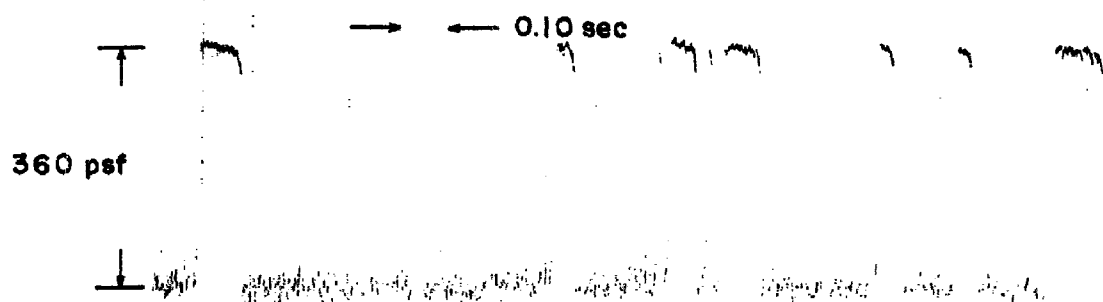


d. $\theta_N = 30 \text{ deg}$

Fig. 12 Concluded

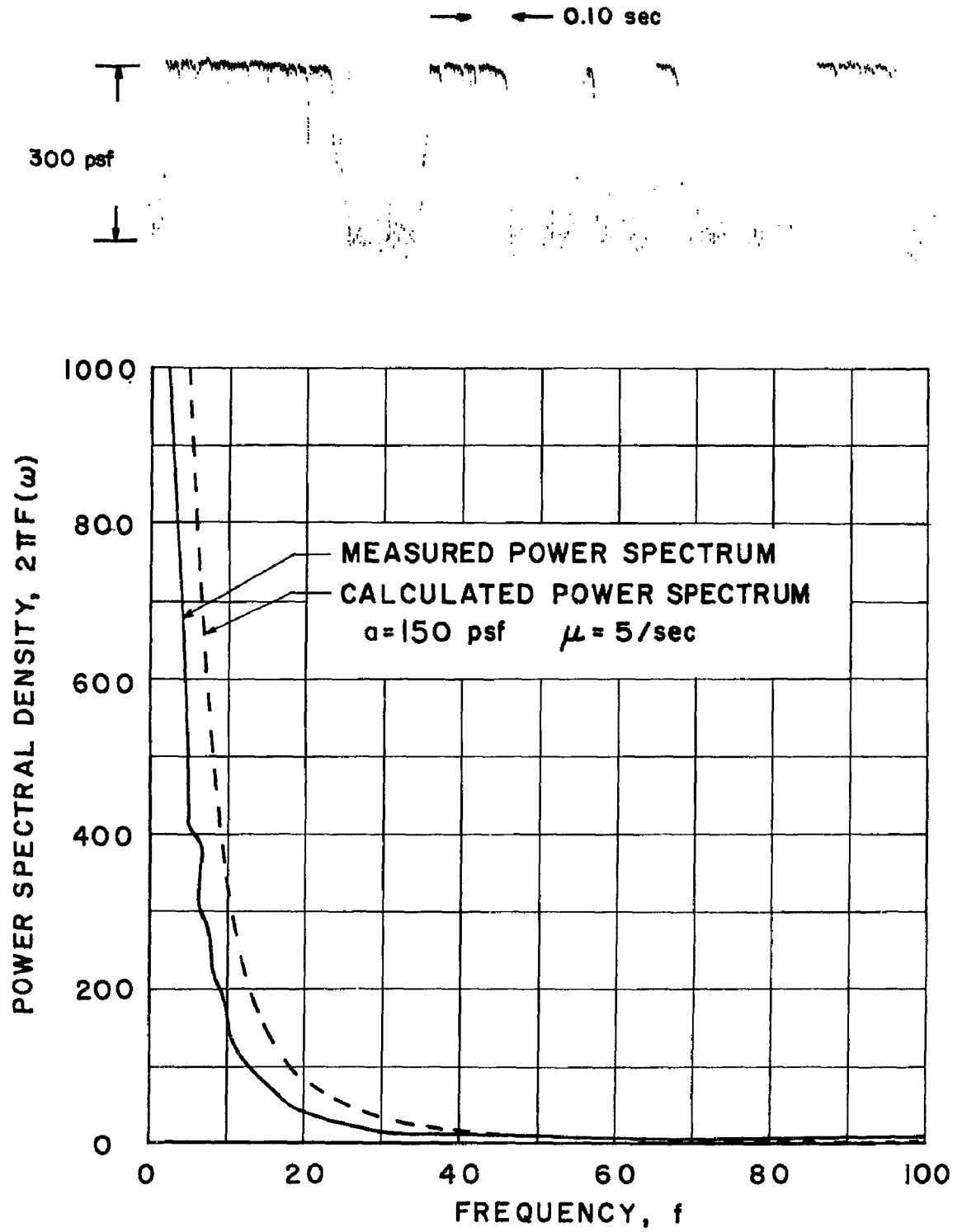


a. $\theta_N = 20$ deg, $\alpha = 0$, $M_\infty = 0.87$
 Fig. 13 Power Spectral Densities and Oscillograph Records of the Pressure Fluctuations
 at $x/D = 0.10$



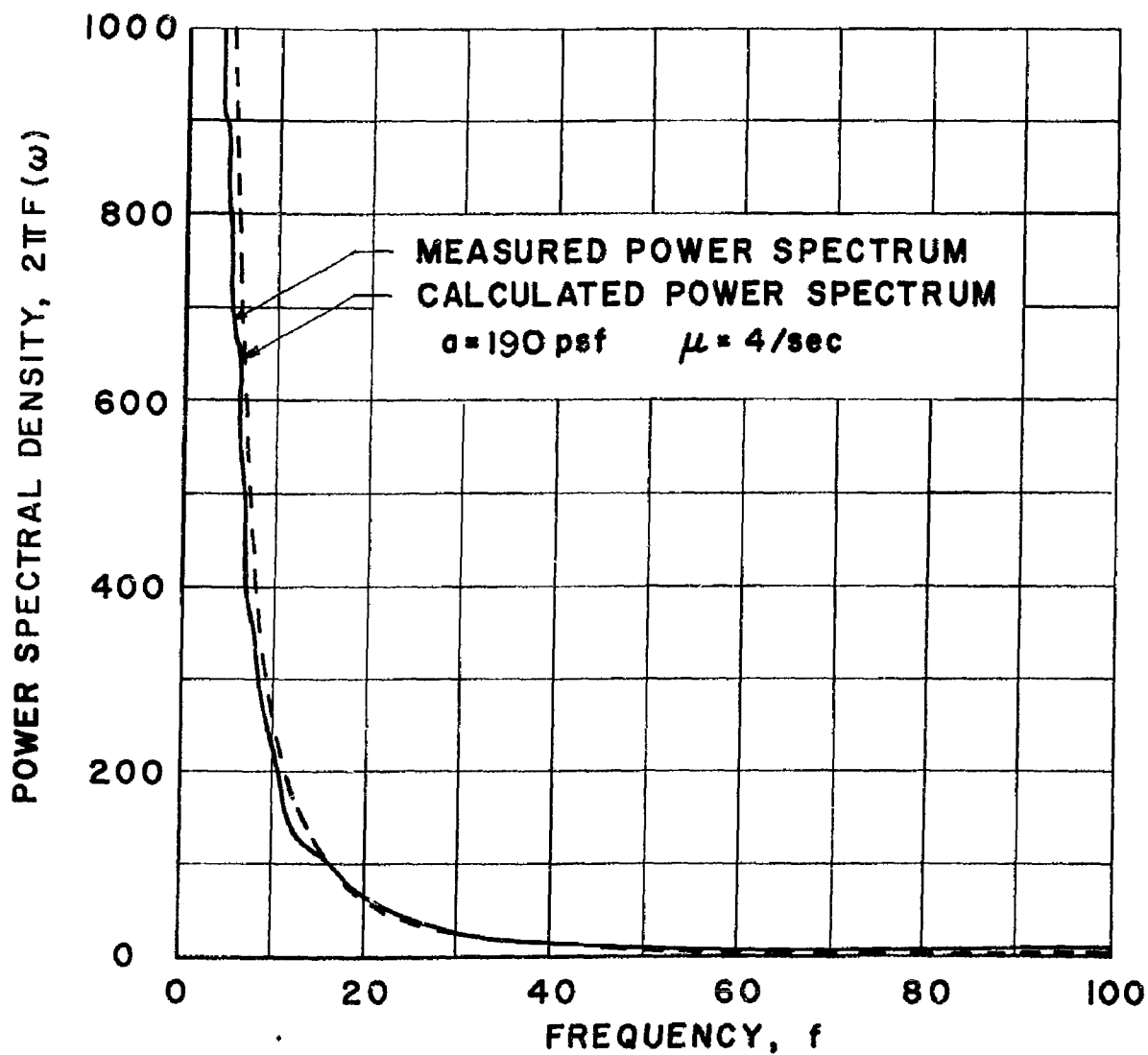
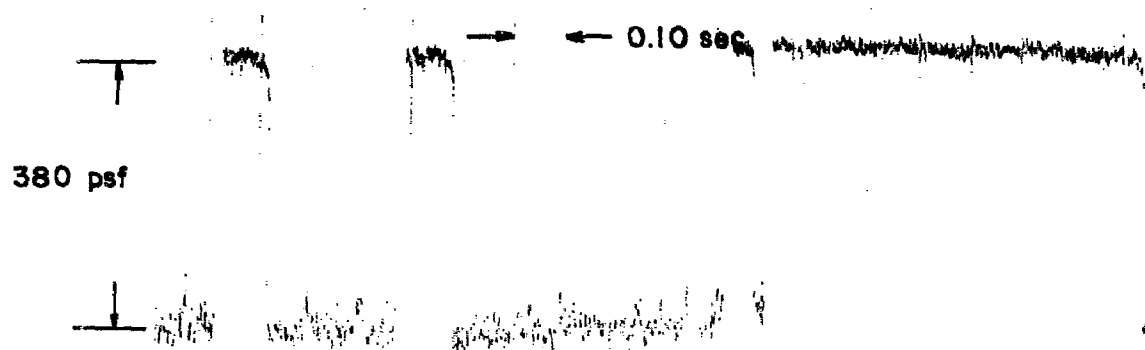
b. $\theta_N = 25$ deg, $\alpha = -2$ deg, $M_\infty = 0.88$

Fig. 13 Continued



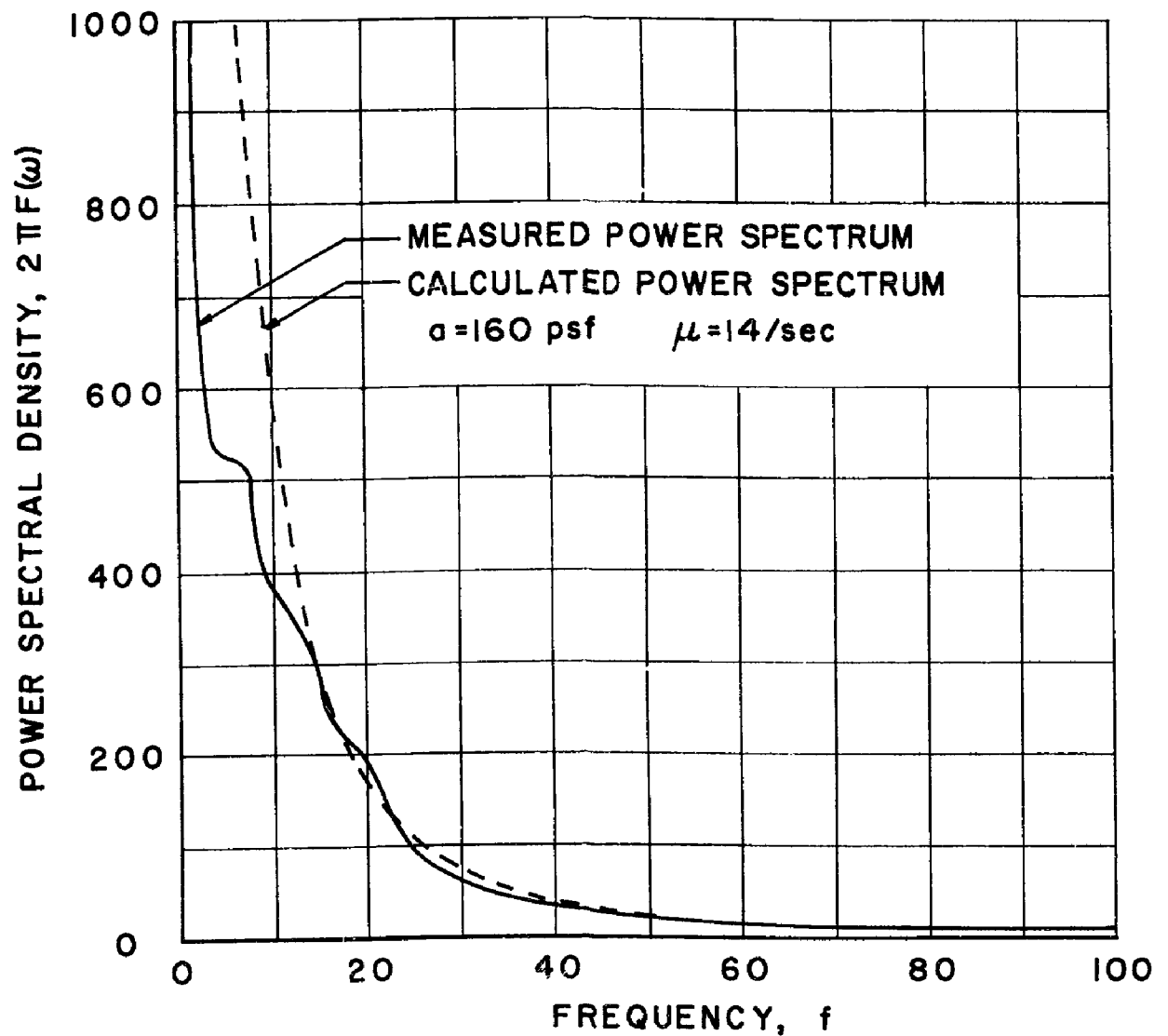
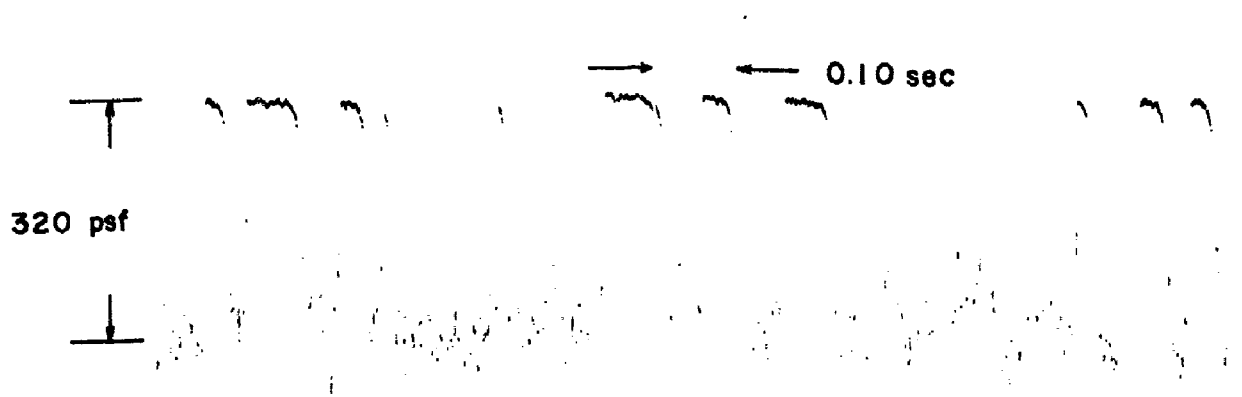
c. $\theta_N = 25 \text{ deg}$, $\alpha = -4 \text{ deg}$, $M_\infty = 0.87$

Fig. 13 Continued



d. $\theta_N = 30 \text{ deg}$, $\alpha = -1 \text{ deg}$, $M_\infty = 0.93$

Fig. 13 Continued



e. $\theta_N = 30 \text{ deg}$, $\alpha = -2 \text{ deg}$, $M_\infty = 0.91$

Fig. 13 Concluded